A Reproduced Copy

OF

Report No. [illegible]

Final Report

DEVELOPMENT OF RADIATION HARDENED LITHIUM-DOPED SOLAR CELLS

July 1969

JPL 952248

Prepared by

D. L. Kendall
R. A. Vineyard
TEXAS INSTRUMENTS INCORPORATED
P. O. Box 5012
Dallas, Texas 75222

for

Jet Propulsion Laboratory
California Institute of Technology
Pasadena, California

Report No. 03-69-37

Final Report

DEVELOPMENT OF RADIATION HARDENED LITHIUM-DOPED SOLAR CELLS

July 1969

JPL 952248

Prepared by

D. L. Kendall
R. A. Vineyard
TEXAS INSTRUMENTS INCORPORATED
P. O. Box 5012
Dallas, Texas 75222

This work was performed for the Jet Propulsion Laboratory, California Institute of Technology, as sponsored by the National Aeronautics and Space Administration under Contract NAS7-100.

ABSTRACT

The results of a year's study on lithium diffused silicon solar cells are presented. Two basic fabrication techniques were utilized on 600 1 X 2 cm cells shipped to JPL as 10 lots of 60 cells each. Variables investigated on the lots included lithium diffusion cycle and silicon crystal types (*Lopex**, Float-zoned and Czochralski). The solar cells were tested for conversion-efficiency, short-circuit current and open-circuit voltage under both tungsten and filtered-xenon light sources. Conversion efficiencies on lots 8, 9 and 10 averaged $> 12.5\%$ under the tungsten light source calibrated at 100 mW/cm^2 sunlight equivalent intensity. Sample cells from lot 5 averaged 10.4% AM0 under the filtered-xenon solar simulator. Although lithium is generally observed in silicon as the interstitial donor, lithium substitutional acceptors were identified and their concentrations measured. Heavily boron-doped silicon ($5 \times 10^{19} cm^{-3}$) was compensated by lithium and the resultant resistivity (apparent) was determined as a function of time. The electrical characteristics (Hall mobility, lifetime, etc.) of lithium-diffused silicon were measured. Impurity diffusion in silicon is reviewed with respect to solar cell characteristics and radiation damage.

* Trademark of Texas Instruments Incorporated.

TABLE OF CONTENTS

LIST OF ILLUSTRATIONS

LIST OF TABLES

SECTION I

INTRODUCTION

In a previous contract report[1] (Contract No. NAS5-10274), technological aspects of making Li-diffused Si solar cells were emphasized, and some of the major problem areas were identified. In this report an attempt to fabricate an optimum cell in terms of a high initial efficiency and improved tolerance to charged particle irradiation was made. Cells were designed to minimize or eliminate the redegradation phenomena observed on many of the initial lithium cells fabricated. Analysis results of the recovery data of the cells showed that the redegradation was due primarily to excessive Li concentrations near the outer edge of the cell. Furthermore, there was an unrecoverable type of damage associated with the complete lack of Li on the extreme edges of the cell. These conditions were remedied by an approach that will be discussed later. However, as a preface to this and to provide useful background material, extractions of several sections relevant to solar cells and radiation damage from an extensive review article[2] on Si diffusion prepared by D. L. Kendall and Dale De Vries on a Company-sponsored program are included in this report. The article was presented at the Material Science and Technology Symposium, sponsored by the Electrochemical Society, on May 4, 1969 in New York. The quantitative defect and diffusion models presented will be useful from a theoretical standpoint and should serve as good working hypotheses for the state of affairs that exists during high temperature operations and during the cooling cycle. These models may also be important when considering annealing of Li-diffused solar cells after irradiation.

SECTION II

TECHNICAL DISCUSSION

A. DIFFUSION IN SILICON

Over the past 15 years, a great deal of data have been taken regarding impurity diffusion in Si. The results of a critical review[2] of the published literature concerned with impurity and self-diffusion with the intent of recording the important points in quickly accessible form are presented here. Figure 1 and Appendix A are a tabulation of the published data. The references cited in the tables of Appendix A are listed separately.

Data for the diffusion of 27 different impurities are tabulated in Appendix A. The diffusion coefficients believed to be characteristic of the lowest impurity concentrations are underlined in Appendix A and are shown in Figure 1. The concentration dependence of several of these impurity diffusion coefficients is quite significant.

Figure 2 is a graphical solution for the solubility of various vacancy-type defects as a function of Fermi level at 1090°C. The defect energy levels used for this calculation are those shown in Figure 3. The levels further are assumed to maintain their same relative position in the gap at 1090°C as those shown at 0°K. The enhanced solubility of these defects at high concentrations is probably responsible for most of the deviations from ideality observed in high concentration boron and phosphorus diffusion profiles. These same defects are probably also responsible for the extremely short minority carrier lifetimes observed in the diffused layers of solar cells. The graphical approach of Figure 2 is that of Shockley and Moll[3], although modified to account for Fermi statistics. Kroger[4] has a good discussion of the chemical approach for this same calculation. The divacancy (W) and monovacancy (V) concentrations shown are only relative, both about three orders of magnitude higher than estimated. The E-center concentration (phosphorus-vacancy pair) may indeed be as high as that shown (according to preliminary calculations).

Finally, a quantitative defect and diffusion model for Si is shown below that is consistent with a wide range of experimental observations and theoretical calculations. This model implicates the vacancy pair or divacancy as the prime mover of substitutional atoms in Si at high temperatures. Formation energies for both divacancies and simple vacancies are calculated which are consistent with various theoretical estimates. Estimates of divacancy and monovacancy concentration at the melting point and at 1100°C are shown in Table I.

The diffusion coefficient of the divacancy (W) is given by

$$D_W = 6.2 \times 10^{-3} \exp(-1.3/kT) \ cm^2 sec^{-1} \qquad (1)$$

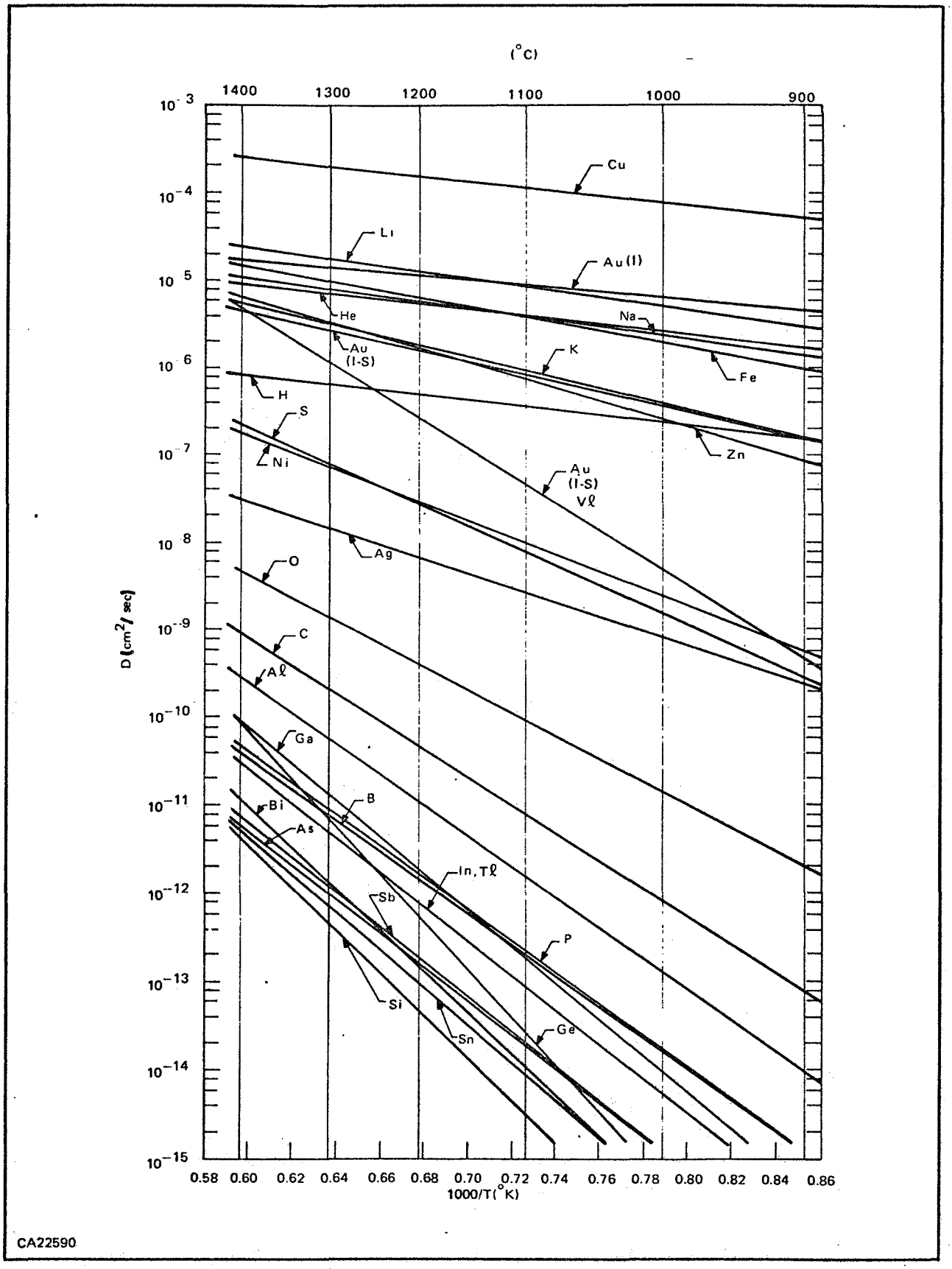

Figure 1. Diffusion Coefficients in Silicon

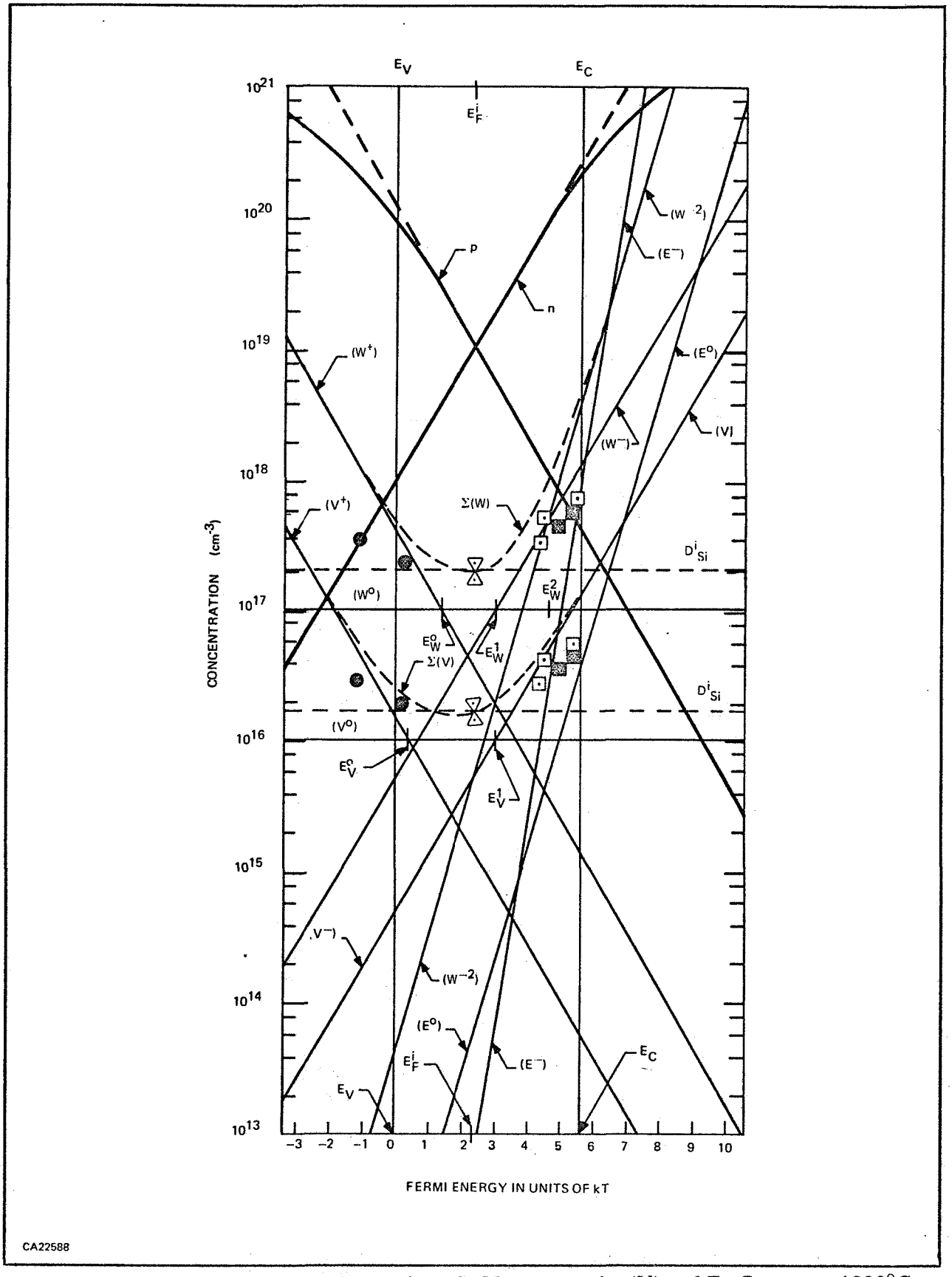

Figure 2. Solubility Plot for Divacancies (W), Monovacancies (V), and E - Centers at 1090°C

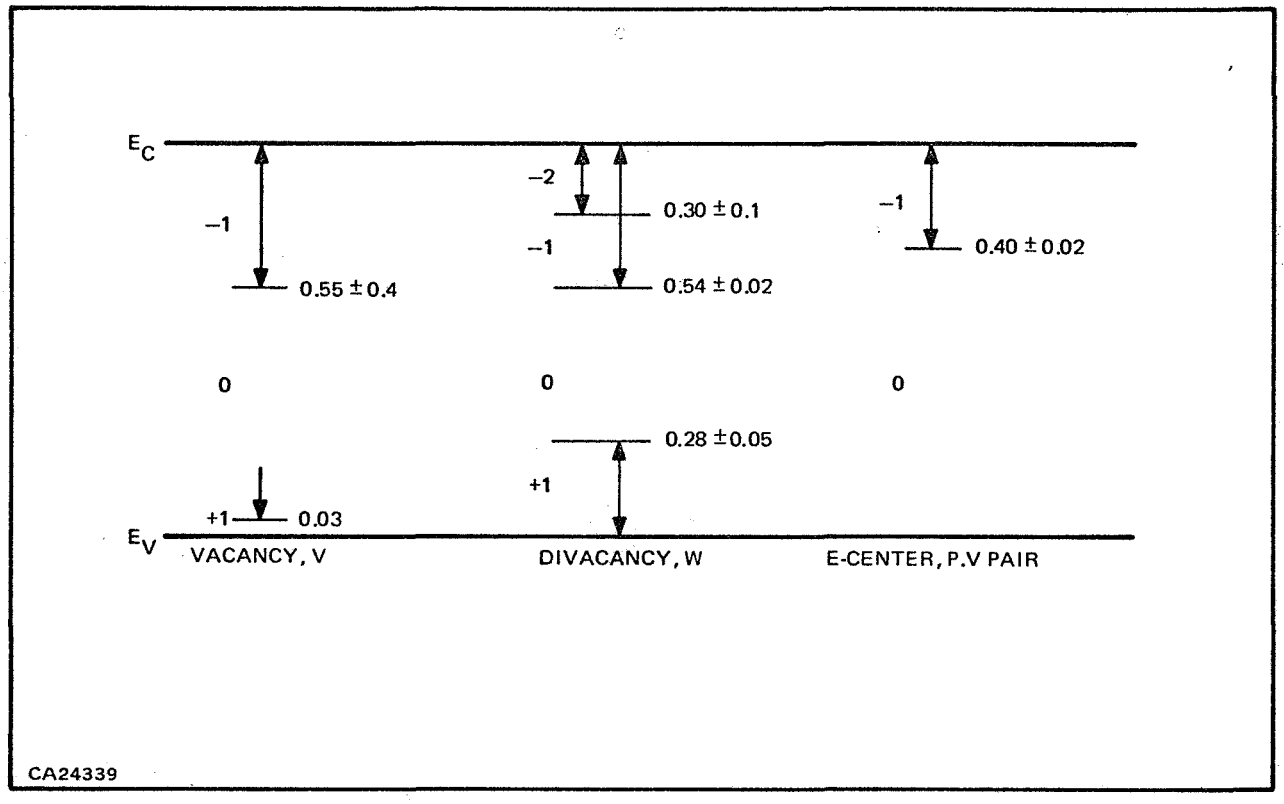

Figure 3. Energy Levels of 0°K for Vacancy Containing Species in Silicon

Table I. Defect Diffusion Coefficients and Concentrations in Silicon Assuming Two Different Mechanisms for Self-Diffusion in Silicon at High Temperatures

Mechanism		Temperature	
		1412°C	1100°C
Divacancy	D_W ($cm^2 sec^{-1}$)	7.8×10^{-7}	1.0×10^{-7}
	N_W (cm^{-3})	5.0×10^{16}	2.1×10^{14}
	D_V ($cm^2 sec^{-1}$)	7.3×10^{-5}	4.4×10^{-5}
	N_V (cm^{-3})	1.4×10^{15}	2.6×10^{13}
Extended Vacancy	D_{V_e} ($cm^2 sec^{-1}$)	7.3×10^{-5}	4.4×10^{-5}
	N_{V_e} (cm^{-3})	6.3×10^{15}	6.1×10^{12}

The divacancy concentration is

$$N_W = 1.2 \times 10^{27} \exp(-3.47/kT) \text{ cm}^{-3} \quad (2)$$

Assuming the divancancy is responsible for silicon self-diffusion at high temperatures (above 1100°C), the monovacancy (V) concentration is calculated to be

$$N_V = 5 \times 10^{22} \exp(-2.53/kT) \text{ cm}^{-3} \quad (3)$$

The diffusion coefficient of the monovacancy is given by

$$D_V = 7.3 \times 10^{-4} \exp(-0.33/kT) \text{ cm}^2 \quad (4)$$

On the other hand, if a monovacancy mechanism is used to explain the silicon self-diffusion results, the monovacancy must be thought of as disturbing the lattice over many lattice sites. Thus the term "extended vacancy" is applied to such a defect and denoted as V_e. On such a model, which is thought to be less likely than the divacancy model, the extended vacancy concentration is given by

$$N_{V_e} = 1.2 \times 10^{29} \exp(-4.44/kT) \text{ cm}^{-3} \quad (5)$$

and the diffusion coefficient is assumed to be the same as the simple monovacancy above (Equation 4).

The self-diffusion data of Peart[5] were used in the above analyses, although the data of Masters and Fairfield[6,7] and Ghoshtagore[8] lead to very similar predictions. The analysis is based, to a significant degree, on the spin resonance work of Watkins[9] and is very similar to the treatments of Kendall[10] and Ghoshtagore[11].

B. LITHIUM DIFFUSION TECHNIQUES

1. Evaporated Lithium

The technique emphasized in our cell manufacture is the use of pure evaporated lithium on side A of a chemically or mechanically polished slice where side B has already been diffused with boron. The latter p+ layer is quite heavily doped ($\approx 10^{20}$ cm^{-3}) and acts as an infinite sink for the interstitial donor lithium arriving from side A, at least for the early parts of the diffusion run. Eventually, however, this p+ layer will reach a point where it is no longer an effective sink for the lithium. This is shown schematically in Figure 4.

This situation will be maintained until the integrated atom flux crossing the junction (x_j) becomes comparable to the maximum amount of lithium that can be put into the boron-doped layer. To estimate this, a 10^{-4}cm thick p-layer and an average lithium concentration of 10^{20} cm^{-3} in this layer was chosen. This permutes into an integrated concentration, $Q_{max} = 10^{16}$ cm^{-2}. The maximum flux across the silicon slab occurs when $\Delta(\text{Li})/\Delta X$ = a constant, which is represented by the linear gradient of Figure 4. Assuming a solar cell slice thickness of 0.03 cm and the solid solubility of lithium at the diffusion temperature of 400°C; $\Delta(\text{Li})/\Delta X = -1.2 \times 10^{18}$ cm^{-3}/0.03 cm = -4×10^{19} cm^{-4}. Taking the D value of 2.5×10^{-8} cm^2 sec^{-1} for lithium at 400°C (Appendix A, Reference 71), a minimum saturation time, t_s, to give an integrated flux, Φ, adequate

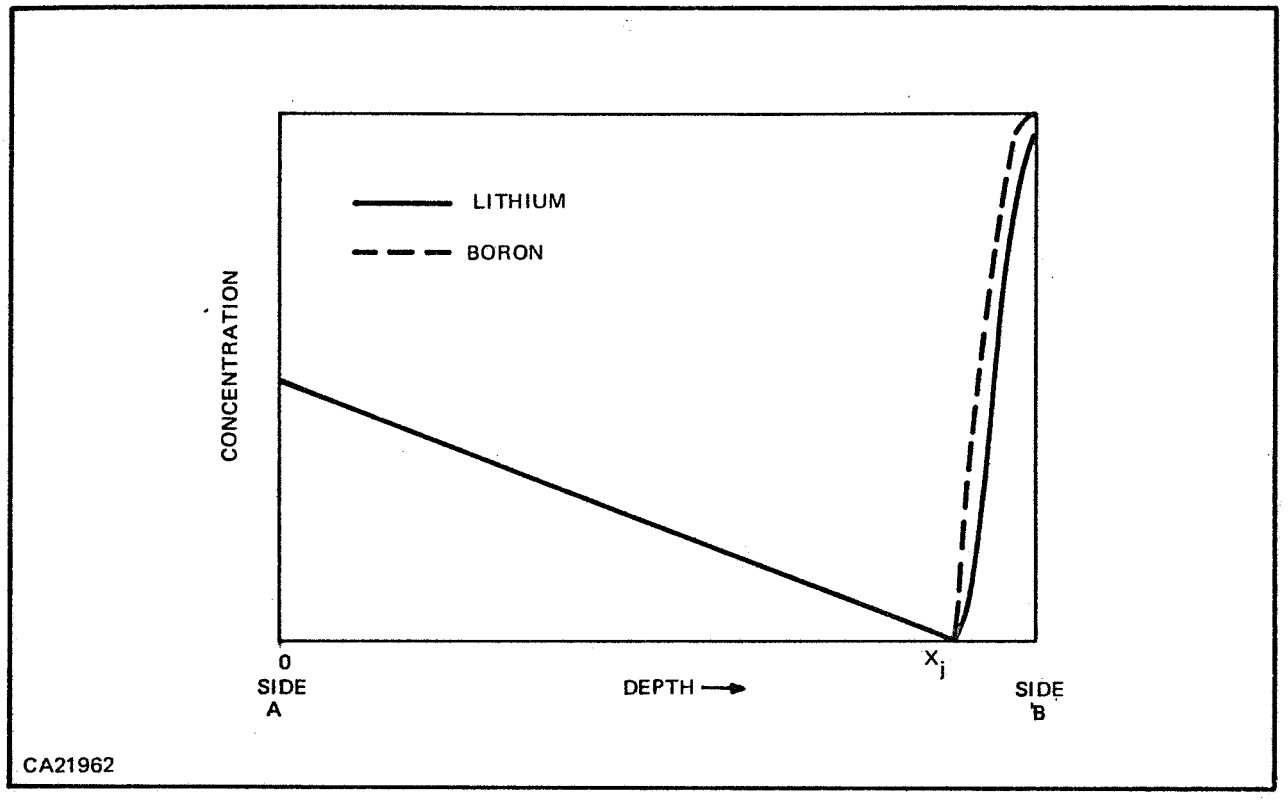

Figure 4. Assumed Lithium Distribution When a Steady State Condition is Reached

to saturate the boron layer with lithium (i.e., to Q_{max}) can be calculated from the following expression:

$$\Phi = Jt_s = -D \frac{\Delta C}{\Delta X} t_s = Q_{max} \tag{6}$$

thus

$$t_s = \frac{Q_{max}}{D\ \Delta C/\Delta X} = \frac{10^{16}}{2.5\ X\ 10^{-8}\ 4\ X\ 10^{19}} = 10^4 \text{ sec} \approx 3 \text{ hours}$$

Since the time used for most of the cells was only 1.5 hours, this is well within the limit. This is especially true when the actual diffusion conditions are taken into account (as shown below) since in the first hour of diffusion at 400°C, almost no lithium crosses the junction, so the above estimate is quite conservative.

The actual profile under constant surface concentration conditions at X = 0 and a permeable boundary at W is given by:

$$\frac{N}{N_o} = 1 - \frac{X}{W} - \frac{2}{\pi} \sum_{n=1}^{\infty} \left[\frac{1}{n} \exp \left(\frac{n^2 \pi^2 Dt}{W^2} \right) \sin \frac{n\pi X}{W} \right] \tag{7}$$

Where N_o is the surface concentration, N is the concentration at any point X and W is the thickness of the slice. (This ignores the p-layer thickness). The other symbols have their classical meanings. A graph of this function at different times at both 325°C and 400°C is given in Figure 5. The D values were 5×10^{-9} and 2.5×10^{-8} cm^2 sec^{-1}, respectively. Note the 325°C curve after 8.0 hours of diffusion is very similar to the 400°C curve at 1.6 hours, the only difference is the lower surface concentration at 325°C (6×10^{17} cm^{-3} instead of 1.2×10^{18} cm^{-3}).

2. Silicon Enclosure Method*

A diffusion scheme was developed that consisted of a "silicon box" approach reminiscent of that used by Miller and Savage (Appendix A, Reference 16) for aluminum diffusion into silicon. This is shown in Figures 6 and 7. The lithium was applied to the carrier slices by evaporation, first permeates the carrier slices, and then crosses the boundary to the sample to be diffused. It was found desirable to heat the slices to 200°C during evaporation and keep them hot while transferring them to the diffusion furnace. This minimized the reaction with air, evidently by not allowing moisture to condense on the hot surface. This approach is evidently limited in its range of application to temperatures greater than about 525°C when diffused in a furnace tube under forming gas. The data in the critical range of temperatures are shown in Table II where ρ_o is the the original P-type resistivity and ρ_f is the resistivity after a given lithium diffusion process. These diffusion runs were in the range 8 to 16 hours. The results did not depend on diffusion time over this range. Note that at 547°C and above, the lithium solubility limit is reached in the samples. The surface damage was negligible in all these cases. At a temperature of 1000°C, there was a tendency for the sample and sample container to stick to the lithium carrier slices. When this occurred, a bluish stain could be seen after separating the slices. This may be due to the formation of an oxide. Runs made in tank-argon were similarly affected.

3. Vapor Diffusion Using a Lithium:Tin Alloy

Cells using the "silicon box" technique with various lithium:tin compositions have been constructed. These were quite irreproducible and additional engineering work needs to be done before this could be utilized as a cell manufacturing method. Therefore, no cells were fabricated by this technique for shipment to JPL on this contract. However, the use of Li:Sn as a diffusion source has some very interesting implications. The Sn:Li system was originally applied to Si diffusion by Reiss and Fuller[12]. However, they used oxidized Si and immersed the samples in a Sn:Li bath. For solar cell manufacture, this is not particularly desirable, so a vapor diffusion scheme using a Sn:Li alloy was attempted. In this case, the Sn acts primarily as a dilutant for the vapor pressure, P_{Li}, or more precisely it modifies the chemical activity of Li, a_{Li}. This quantity is given by

$$a_{Li} = \frac{P_{Li}}{P^{\circ}_{Li}}$$

where P°_{Li} is the equilibrium vapor pressure over pure Li at the given temperature.

* Gregg Lee, who is now serving as an officer in the Air Force, is responsible for most of the experimental work in this section as well as that in C, D, and E.

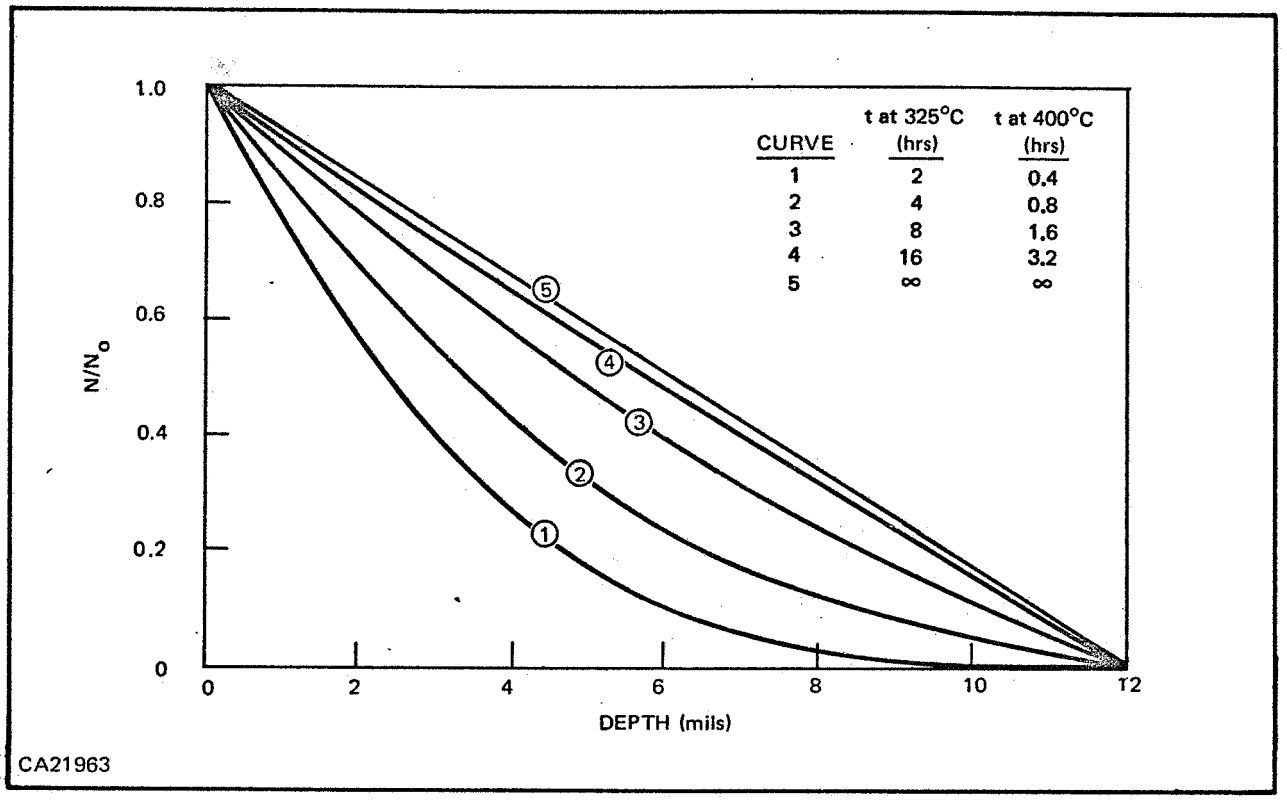

Figure 5. Theoretical Curves for Lithium Diffusion in a Silicon Slice of 12 Mils Thickness at Either 325°C or 400°C (Assuming Source at X = 0 and Sink at X = 12 Mils)

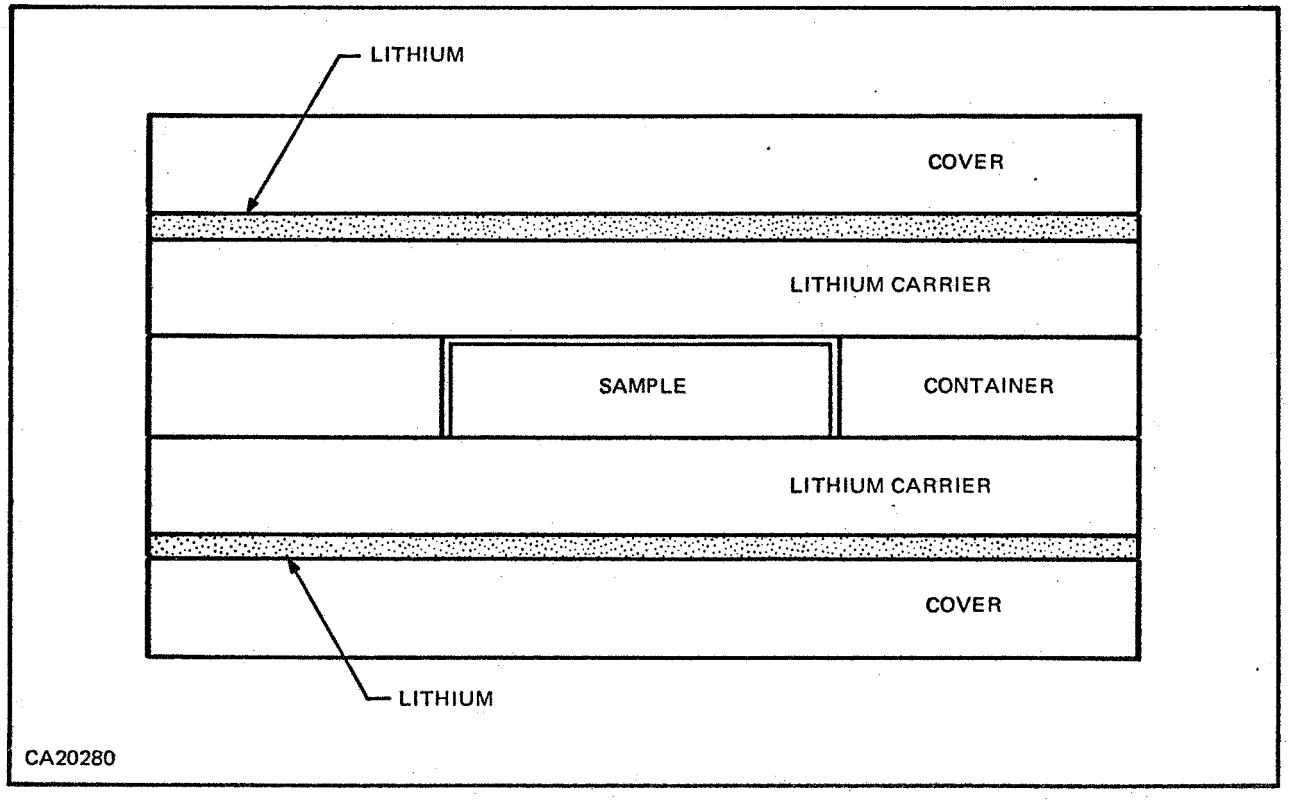

Figure 6. Silicon Box, Longitudinal Section

The activity of Li at 400°C as a function of atomic percent of Li in Sn is estimated in Figure 8 along with the Li:Sn phase diagram[14]. The most interesting features of this graph are the six level regions of chemical activity. In each of these regions, the Li-vapor pressure is constant over a range of composition. For example, in Region 1 this applies from 33 atomic % to 50 atomic % Li. One can then relate the amount of Li introduced into Si to the percentage in the alloy. Over this range of alloy composition at 400°C, the surface concentration of Li in the Si is invariant. Several early runs suggested that the resistivity after diffusion in this range is 0.055 Ω–cm which corresponds to a Li concentration of 2×10^{17} cm^{-3}.

It will be noted that these arguments apply to either vapor diffusion in an ampoule, in a silicon enclosure, or doping with the alloy evaporated on a slice. A quartz ampoule, however, tends to react continuously with the Li in the alloy, thereby depleting the source. A suitably purged system in conjunction with a Si enclosure would probably be effective. Whether the temperature limitation of 525°C mentioned earlier is valid for these Sn:Li diffusions in a Si enclosure is not known.

The upper ranges (2 to 6) will give progressively higher activity (Li concentrations). Raising the temperature will generally increase activity in a given composition range. From the phase diagram (Figure 8), note that at 505°C one would only traverse four two-phase regions. At 325°C he would traverse seven such zones. Data over the phase field at temperatures ranging from 320°C to 510°C would be of great practical use in designing a Li doping experiment for a solar cell, and precise compensation of B-doped Si to a predetermined value.

The work would also be useful in Li diffusion of other semiconductors (Ge, GaAs, GaSb, and others), since the Si concentration in the Li:Sn alloy is small and is assumed to exert a negligible influence on the activity of Li. Assuming this is true, and, if the dissolution of the semiconductor in question is small enough, the results regarding activity can be taken over to other semiconductors with little change.

The activity in range 0 is a continuously varying function of Li composition, so resistivities above 0.055 can be attained. However, one must somehow avoid or surmount the quartz:Li reaction mentioned earlier. The particular shape shown for range 0 is not inviolate but is shown to illustrate a commonly observed effect, namely that the activity often exhibits a linear region in dilute alloys. If the slope of this region is 1 (or −1 as in the present case) the alloy solution is ideal; or put another way, it follows Raoult's Law which is $a_{Li} = P_{Li}/P^{\circ}_{Li} = (Li^{\circ})$, where (Li°) is the atomic fraction of un-ionized Li. It is the neutral species of Li in the Si lattice that is considered to interact with the external Sn:Li phase. If the slope in this region is either greater or less than unity, the behavior follows Henry's Law, which is $a_{Li} = \gamma\ (Li^{\circ})$, where γ is the so-called activity coefficient.

C. ELECTRICAL PROPERTIES OF LITHIUM-DIFFUSED SILICON

Several samples of lithium-diffused silicon of various resistivities were prepared using a lithium:tin alloy source. Before lithium diffusion, the silicon samples were phosphorus-doped N-type with resistivities above 100 ohm-cm. These were fabricated into Hall bars and electrical measurements taken. TI attempted to make both Hall coefficient and lifetime measurements as a

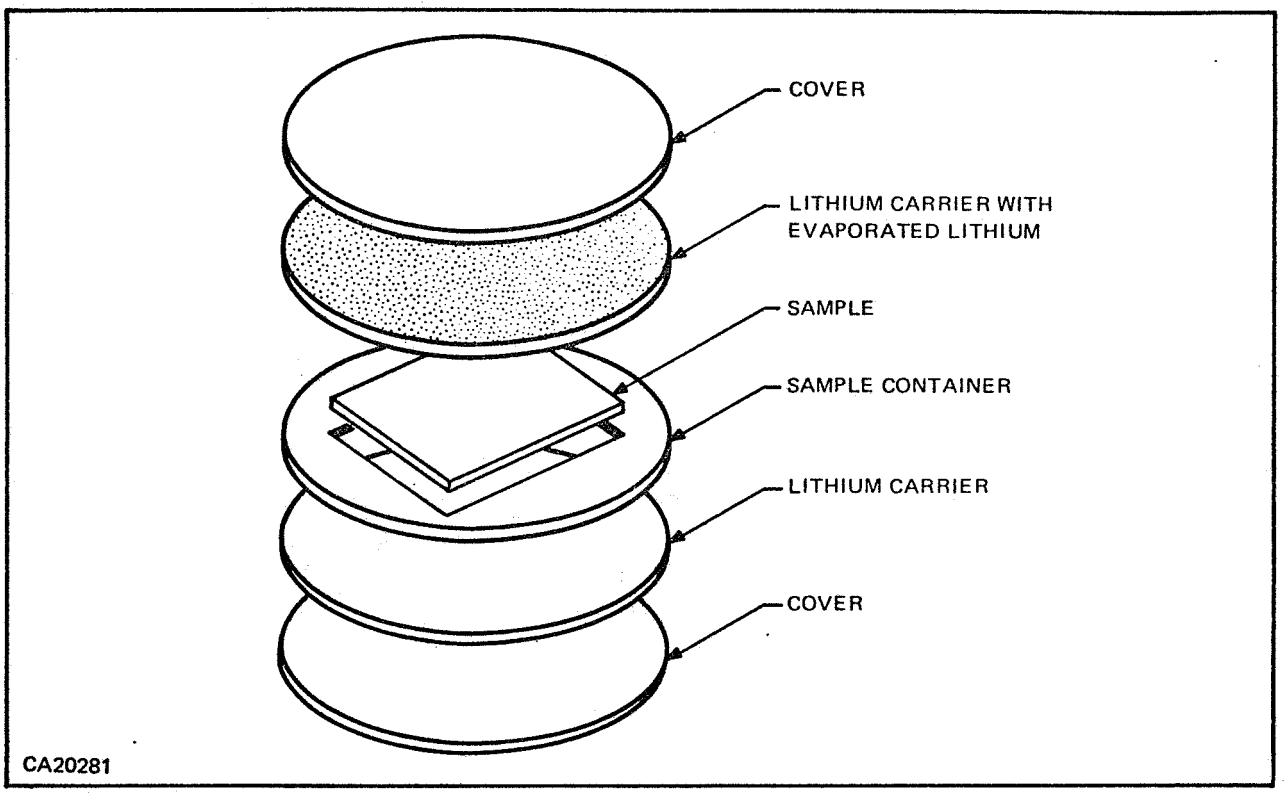

Figure 7. Silicon Box, Exploded View

Table II. Effect of Temperature on Lithium Diffusion in Silicon Box

T (°C)	ρ_o (ohm-cm)	ρ_f (ohm-cm)
400	1.8	1.8 (p)
500	1.8	1.8 (p)
525	1.8	3.5 (p)
547	1.8	0.013 (n)
600	1.8	0.007 (n)

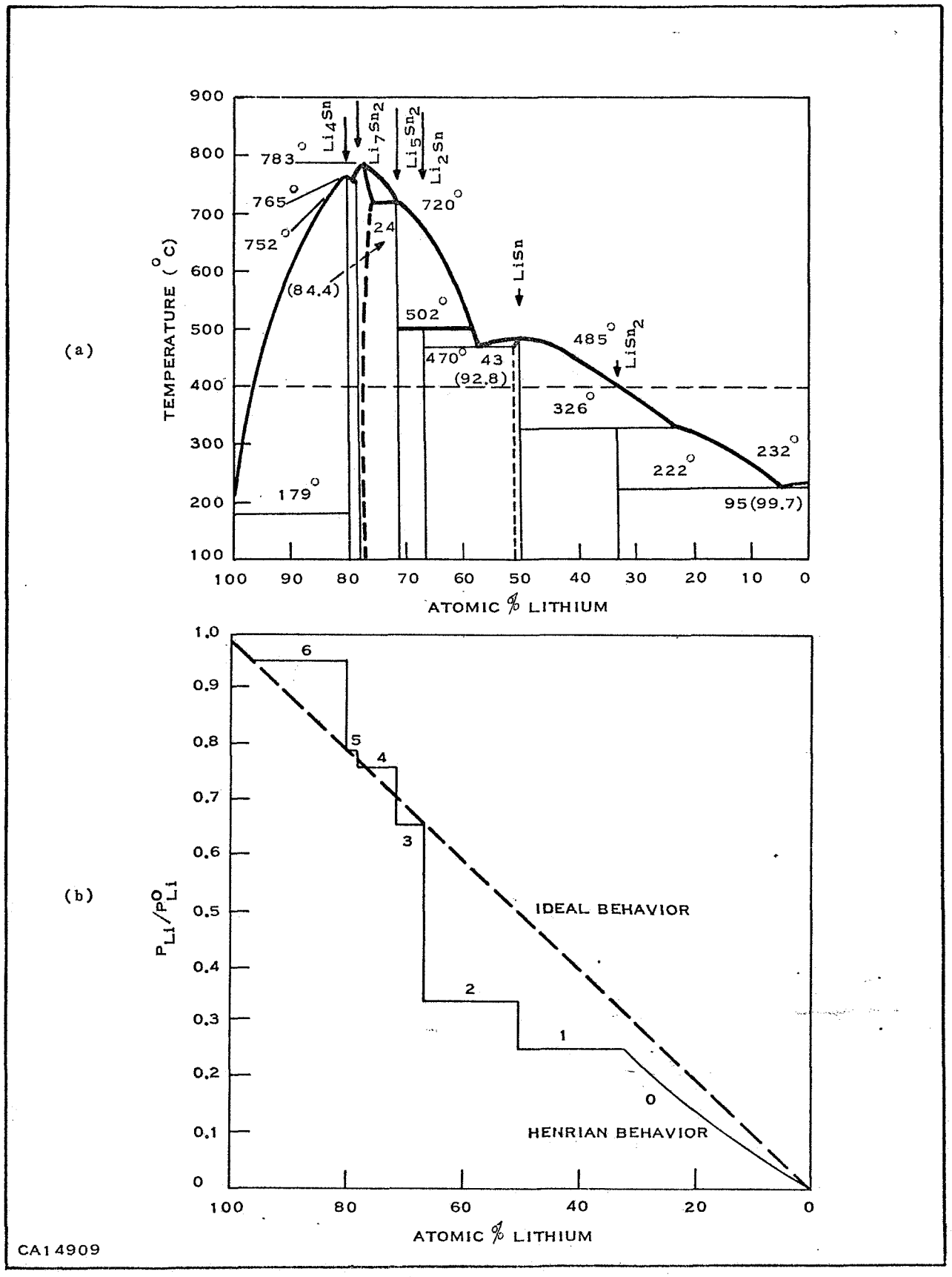

Figure 8. Chemical Activity of Li in an Alloy of Sn on Li as it Relates to Sn:Li Phase Diagram

function of temperature on several of these samples. The Hall measurements are shown in Figures 9 through 12. However, lifetime measurements could not be taken on the samples with the surface photovoltage (SPV) method because the diffusion length was greater than the sample thickness (10 mils). The behavior of the mobility and the carrier concentration over the range of 77° to 300°K is almost identical to that of high-quality arsenic-doped silicon.[16] In view of the different mode of incorporation of lithium (interstitial instead of substitutional), this is not an obvious result. Note also the similarity between the lithium-diffused samples containing oxygen (quartz-crucible QC) and those containing much less of this impurity (*Lopex* L). This is especially evident in samples 75L and 81QC, where a common line has been drawn through the carrier concentration, Hall coefficient, resistivity, and mobility data.

The high quality of the lithium-diffused samples was also evident in the lifetime measurements taken on the first contract.* These data are reproduced in Figure 13. The minority carrier lifetime, τ, exceeds 10 microseconds in all samples containing less than about 2×10^{17} cm^{-3} donors. This corresponds to a minority carrier diffusion length of about 4 mils. If this is adopted as a minimum acceptable lifetime in the active zone of a solar cell, a decision can be made as to whether a given lithium diffusion process will result in a high efficiency solar cell. For example, the cells diffused at 400° for 1.5 hours (Lots T-1 through T-5) should have a profile similar to curve 3 of Figure 5, with a surface concentration at X = 0 of about 1.2×10^{18} cm^{-3}. Thus, near the active solar cell surface (located at X = 12 mils), a region over 3 mils width exists where the lithium is less than 2×10^{17} cm^{-3} and which probably has a τ considerably higher than 10 microseconds. In addition, a rather high Li gradient of about 2.5×10^{19} cm^{-4} exists throughout this region. This is expected to result in a cell that anneals rapidly in a radiation environment.

It was recognized that the above gradient does not exist very near the P-N junction, since both the RCA and TRW groups have shown by C-V measurements of TI cells that the lithium gradient in the first few tenths of mils is somewhat less than that quoted above. This is evidently due to a redistribution process very near the junction that occurs during room temperature storage after the cell is manufactured. This is not surprising since the thin, heavily boron-diffused region will serve as a more effective sink for the lithium donors at room temperature than at higher temperatures, as can be inferred from Figure 14, which is reproduced from the previous contract. However, it is not expected that the lithium in the bulk will continue to diffuse into the boron-diffused layer for very long. This results from an observation by Williams et al.[17] that a thin boron-diffused layer effectively blocks the out-diffusion of lithium from a lithium drifted particle detector. This unexpected result has not been satisfactorily explained, but has been authenticated by several laboratories.

D. LITHIUM COMPENSATION OF BORON-DOPED SILICON

Using the same diffusion method outlined previously, heavily boron-doped silicon (5×10^{19} cm^{-3}) has been compensated by lithium. Reiss and Fuller[12] have previously observed lithium-boron compensation, although they reported no electrical measurements on the compensated material. TI has achieved apparently very exact compensation. Four-point probe readings of apparent resistivity made immediately after the 30 minute lithium diffusion (liquid

* These measurements were taken by Jodie Horak using the SPV method.

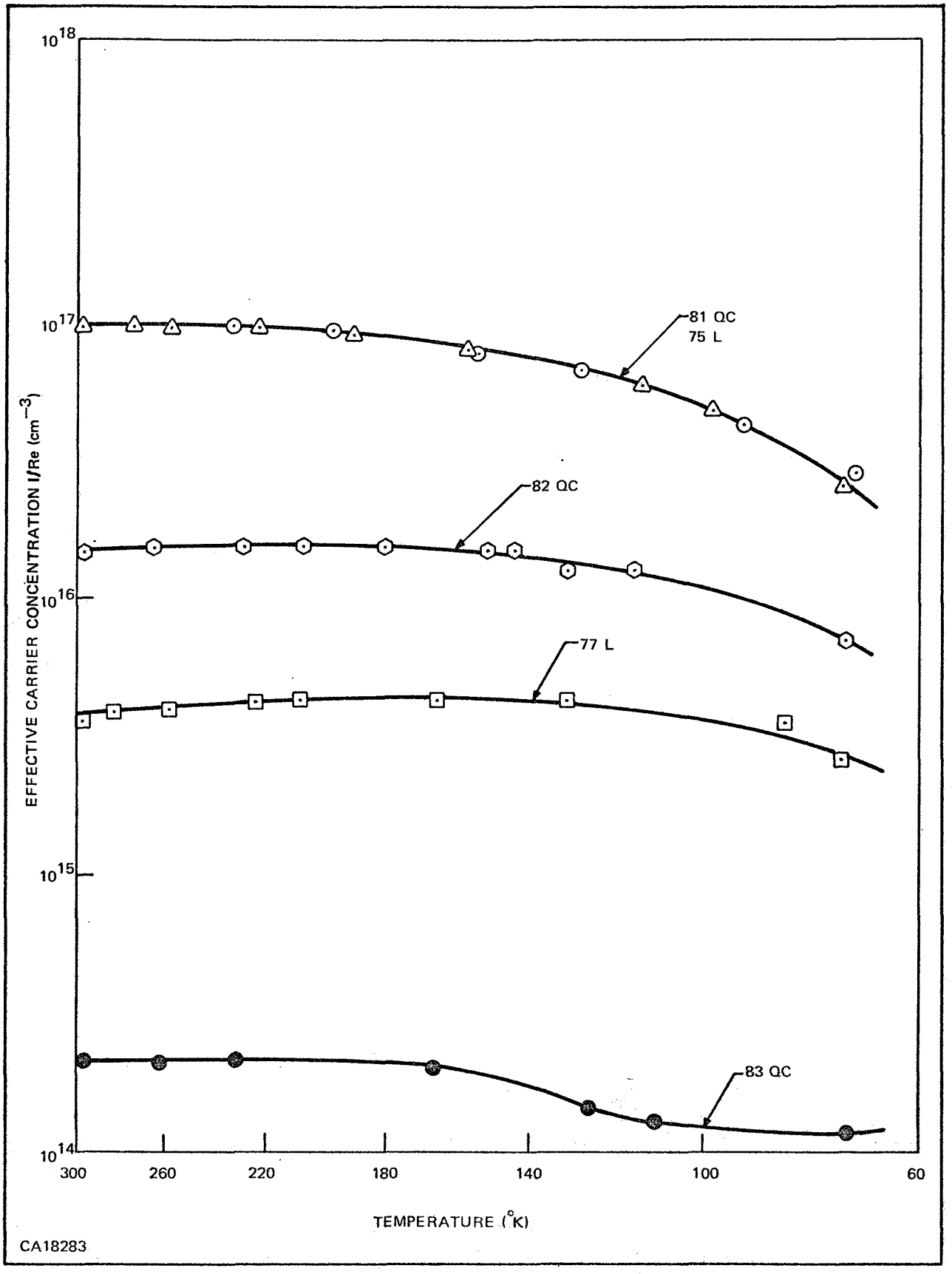

Figure 9. Carrier Concentration versus Temperature for Lithium-Diffused Silicon

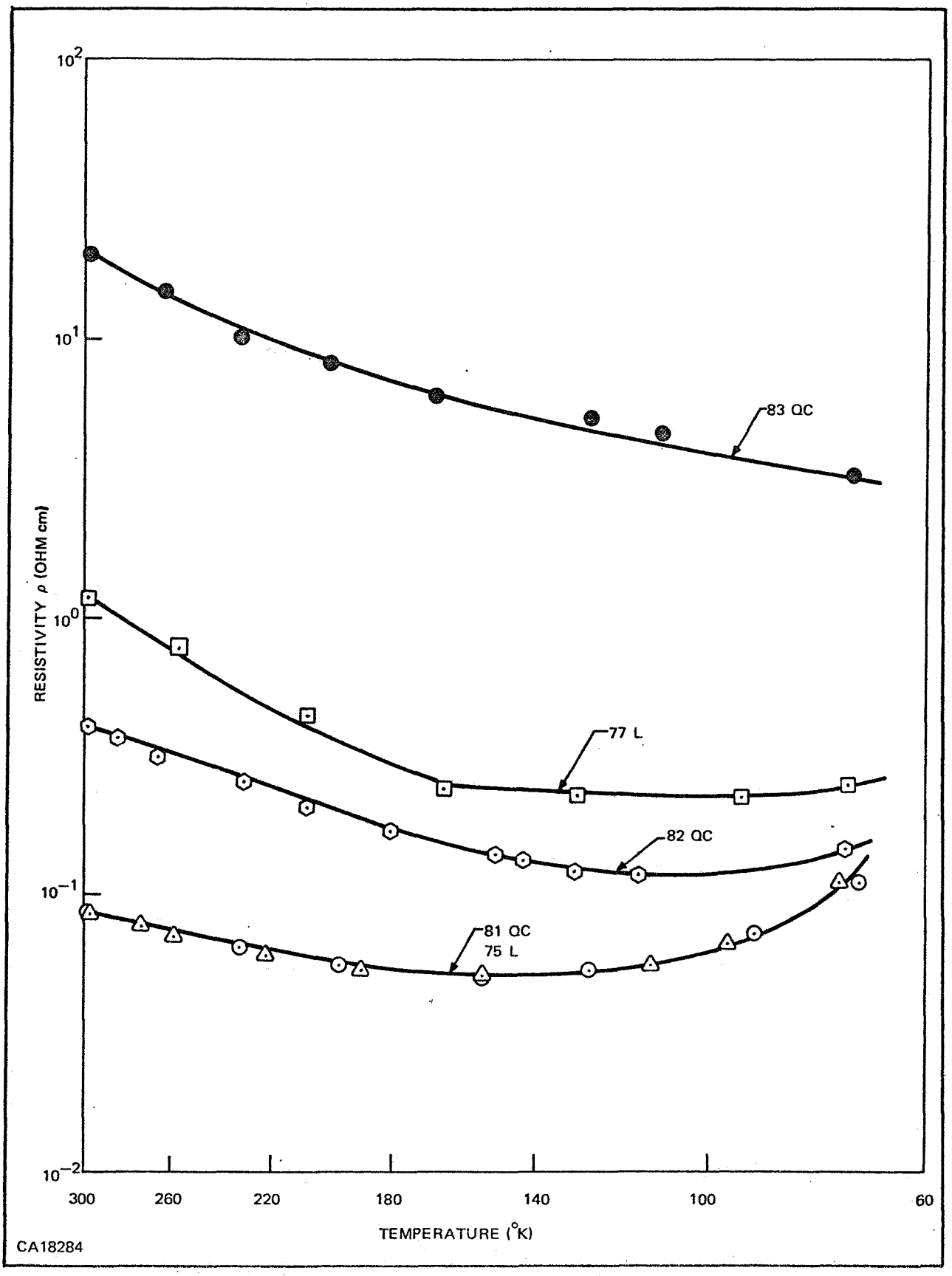

Figure 10. Resistivity versus Temperature for Lithium-Diffused Silicon

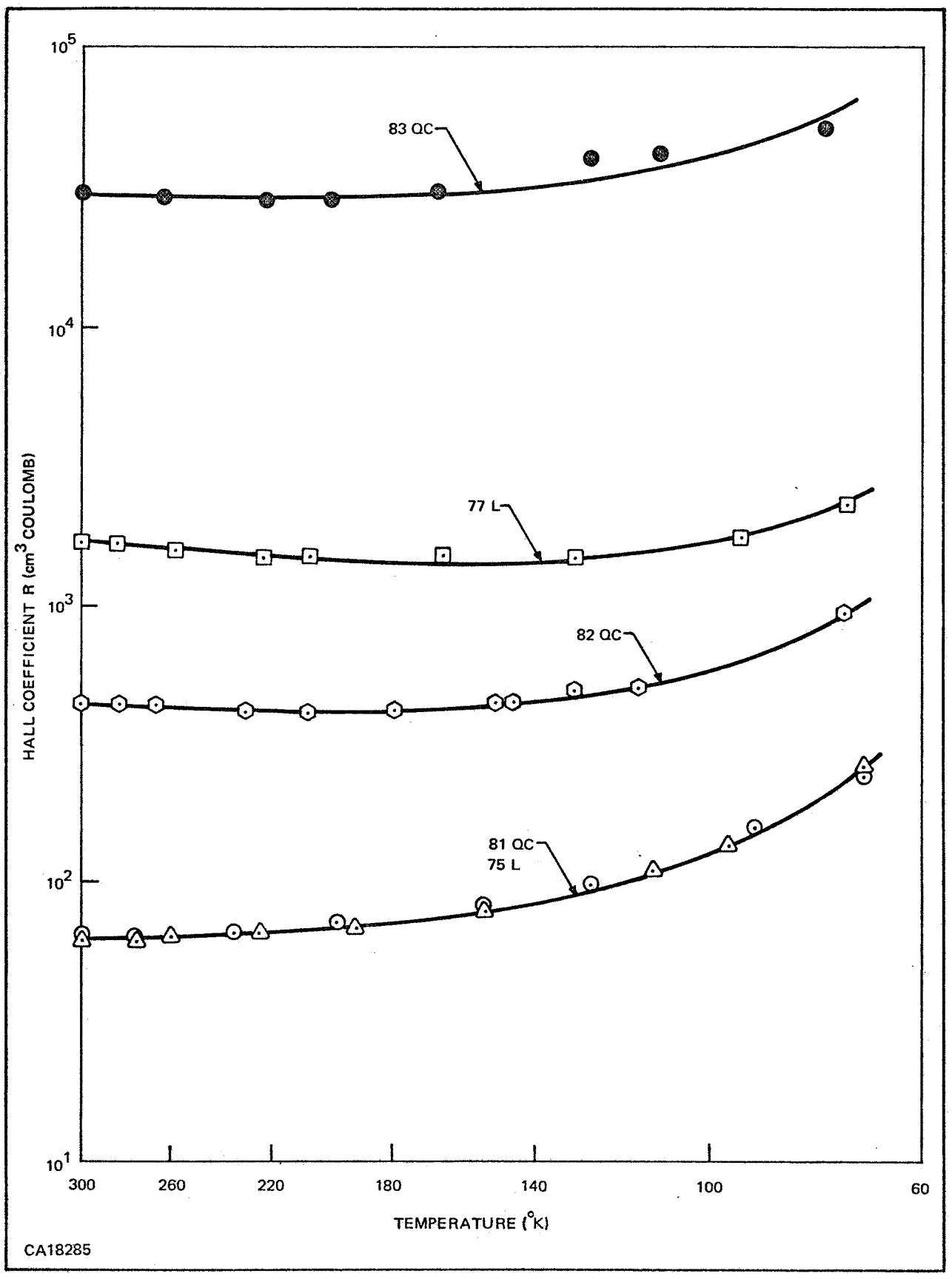

Figure 11. Hall Coefficient versus Temperature for Lithium-Diffused Silicon

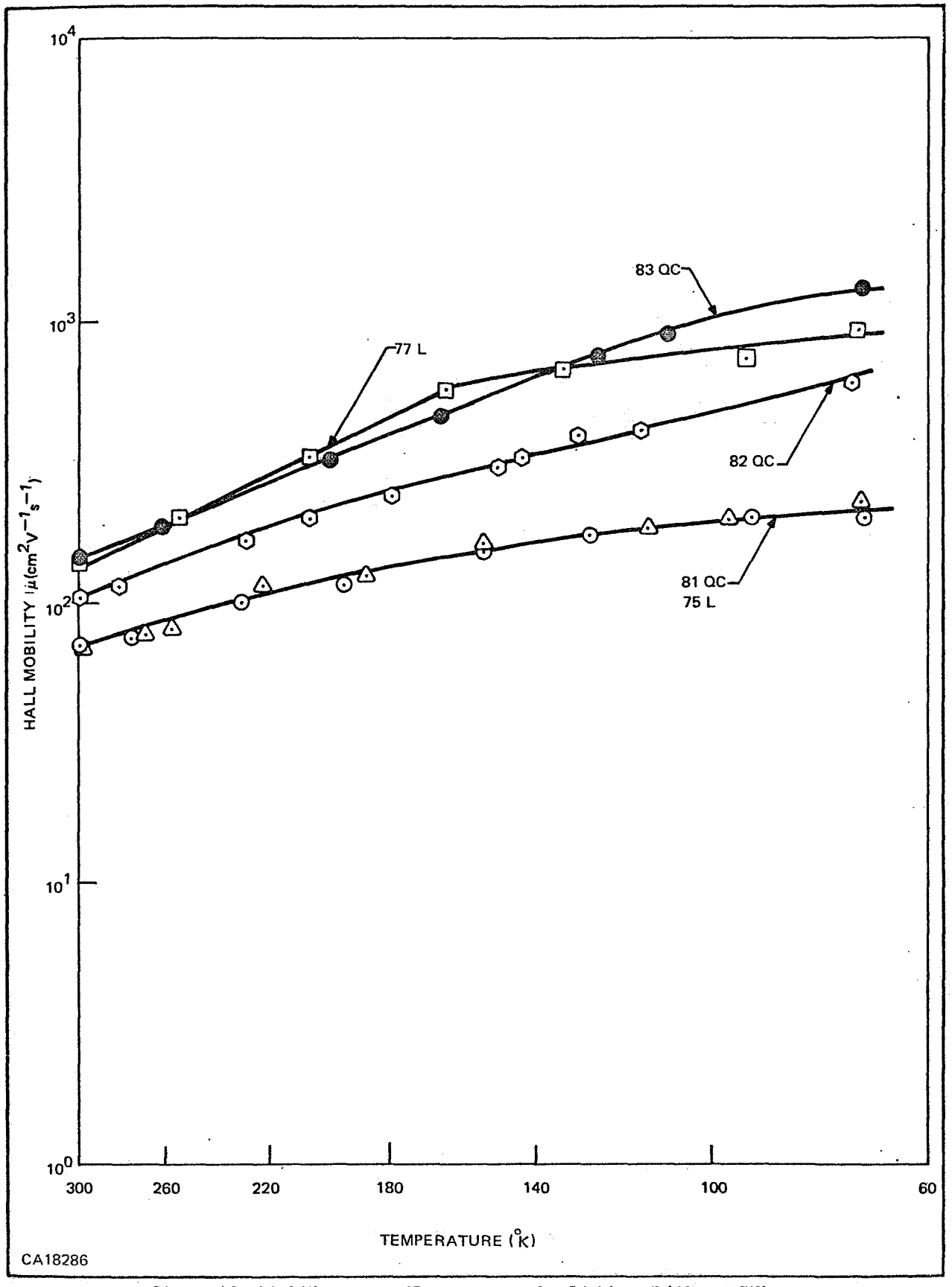

Figure 12. Mobility versus Temperature for Lithium-Diffused Silicon

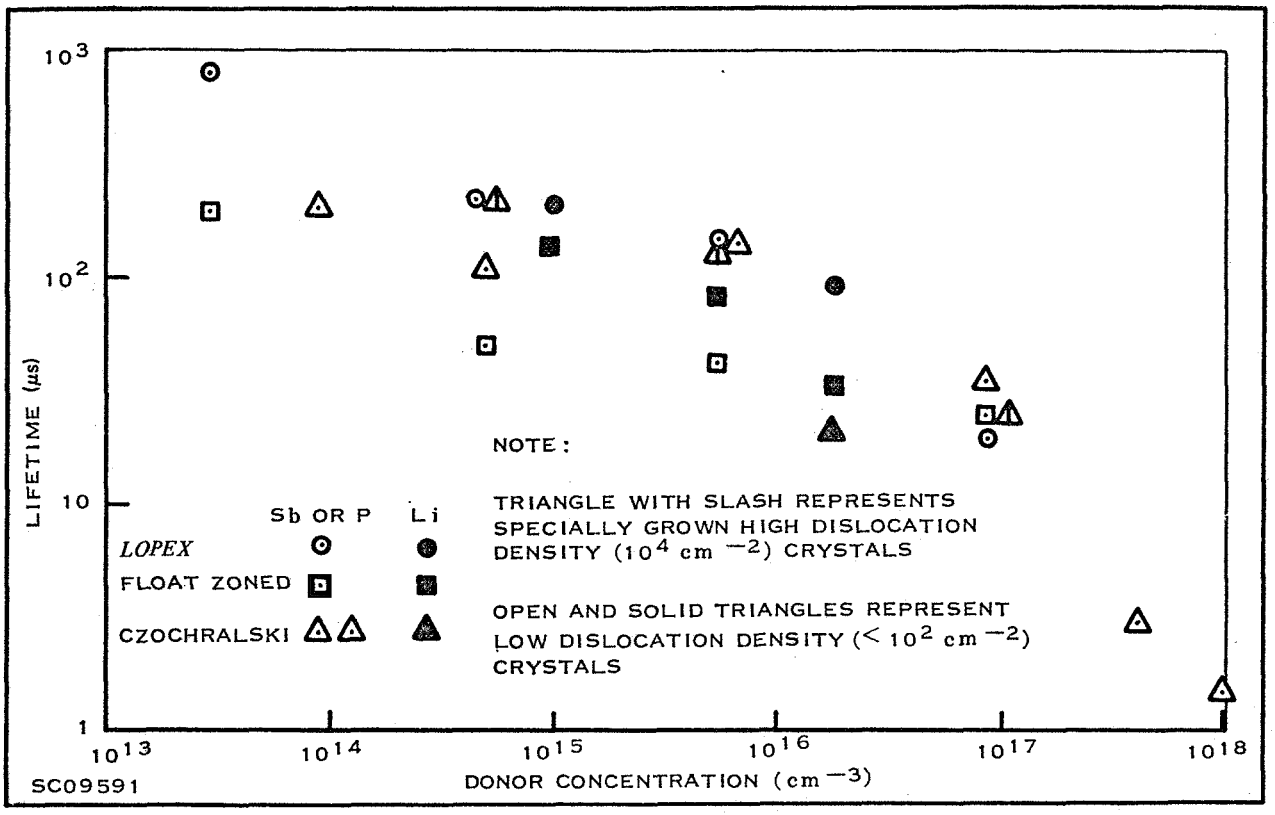

Figure 13. Minority Carrier Lifetime of N-Type Silicon Crystals versus Concentration of Li, Sb, and P

nitrogen quench) ranged from 10^4 Ω-cm to 5 X 10^5 Ω-cm. The apparent resistivity is defined from the geometry of a four-point probe with 10-mil probe spacing to be:

$$\rho = 2\pi s \frac{V}{I} = 0.16 \frac{V}{I} \text{ (Ω-cm)}$$

where

s is the probe spacing
V is the voltage across the two inner probes, and
I is the current between the two outer probes.

In other words, no attempt has been made to correct for thickness of the material being measured.

Readings of apparent resistivity, however, varied with time. After seeming to increase slightly for 3 to 5 minutes, they fell one order of magnitude in 30 minutes and another order of magnitude in 24 hours. Figure 15 is a plot of apparent resistivity versus time for two samples which represent approximately the upper and lower limits of initial resistivity observed. Figure 16 extends the lower curve out to 65 hours after diffusion. Samples which initially are indicated as N-type on a thermoelectric probe change to P-type in the same 3 to 5 minute period that the apparent resistivity seems to rise.

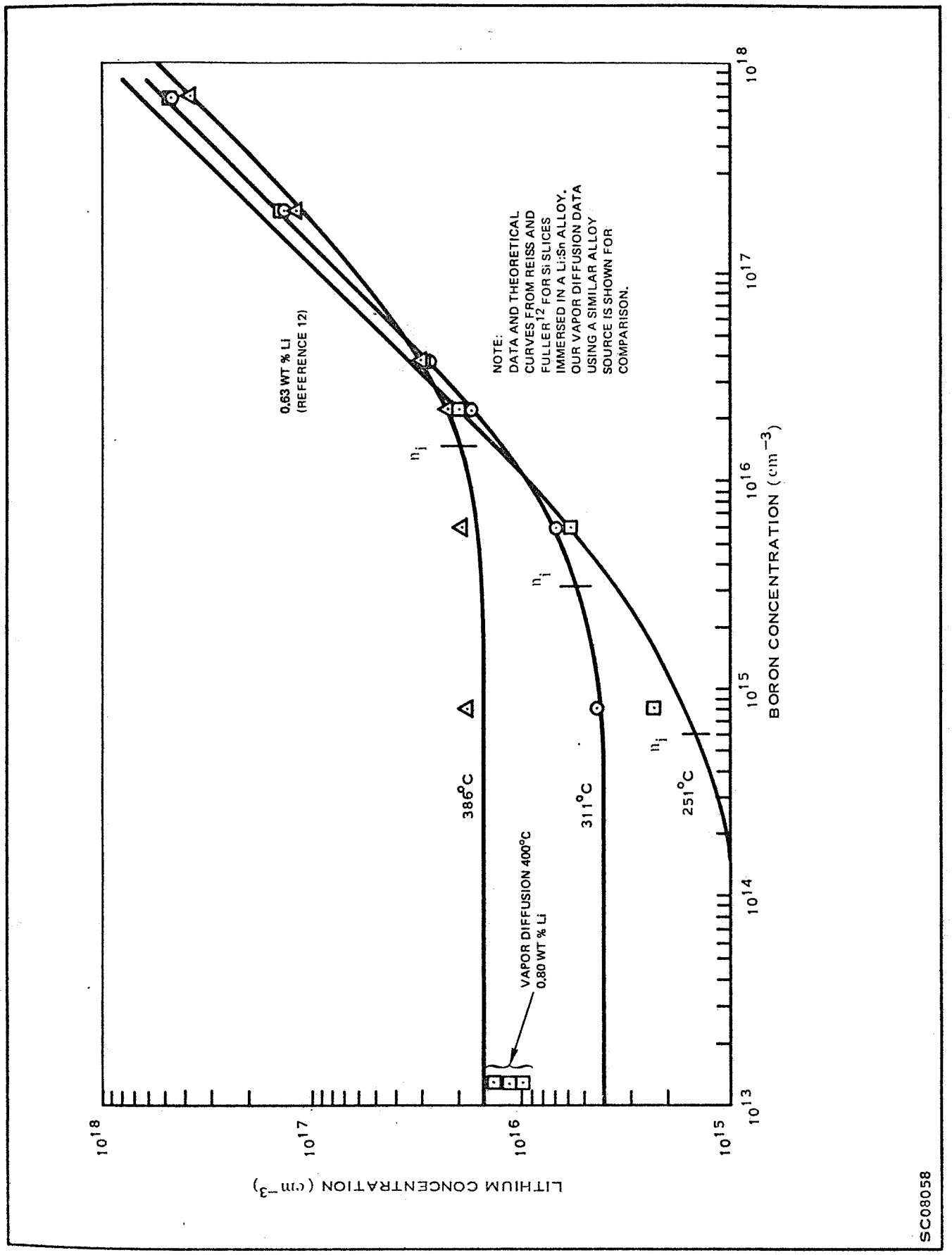

Figure 14. Lithium Saturation Results and the Effect of Boron on Lithium Solubility

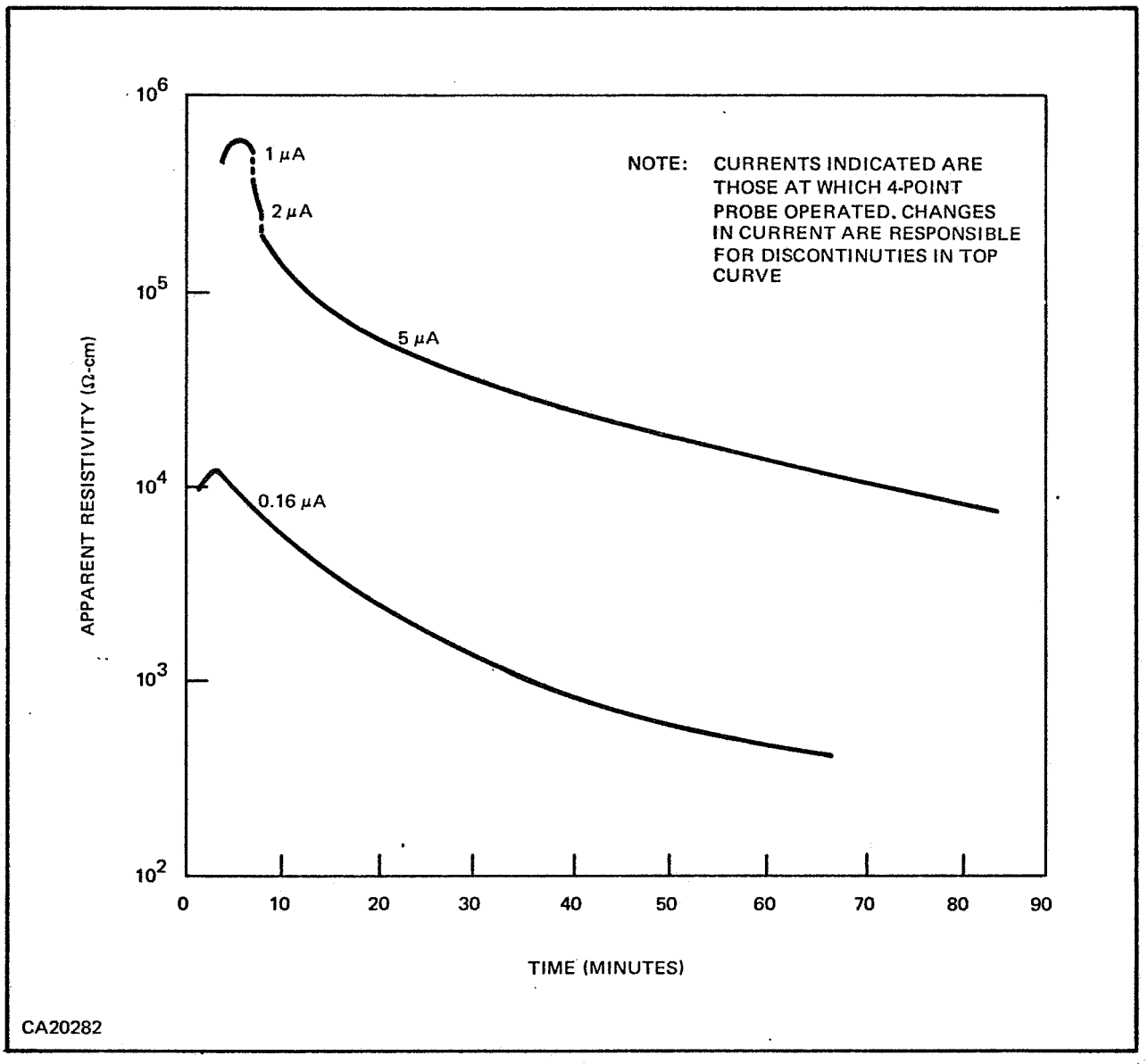

Figure 15. Apparent Resistivity versus Time for Li:B Compensated Samples

This appears to be entirely a surface effect, since lapping the surface on which measurements are being taken will restore the apparent resistivity to the same value observed just after the lithium diffusion. The amount of lapping necessary (approximately 1 mil) to restore the high resistivity is considerably more than can be explained by out-diffusion of lithium to the surface of the material, although this is still the primary suspect as the mechanism involved.

Whether the lithium diffuses to surfaces created by lapping damage or the out-diffusion is somehow enhanced by the presence of boron is unknown, but it is clear that a P-type surface skin develops on the N-type bulk of the samples. The formation of this layer precludes analysis of the electrical properties of the heavily compensated bulk since the P/N junction, as well as the comparatively low resistance of the surface, causes current from measurement equipment to flow

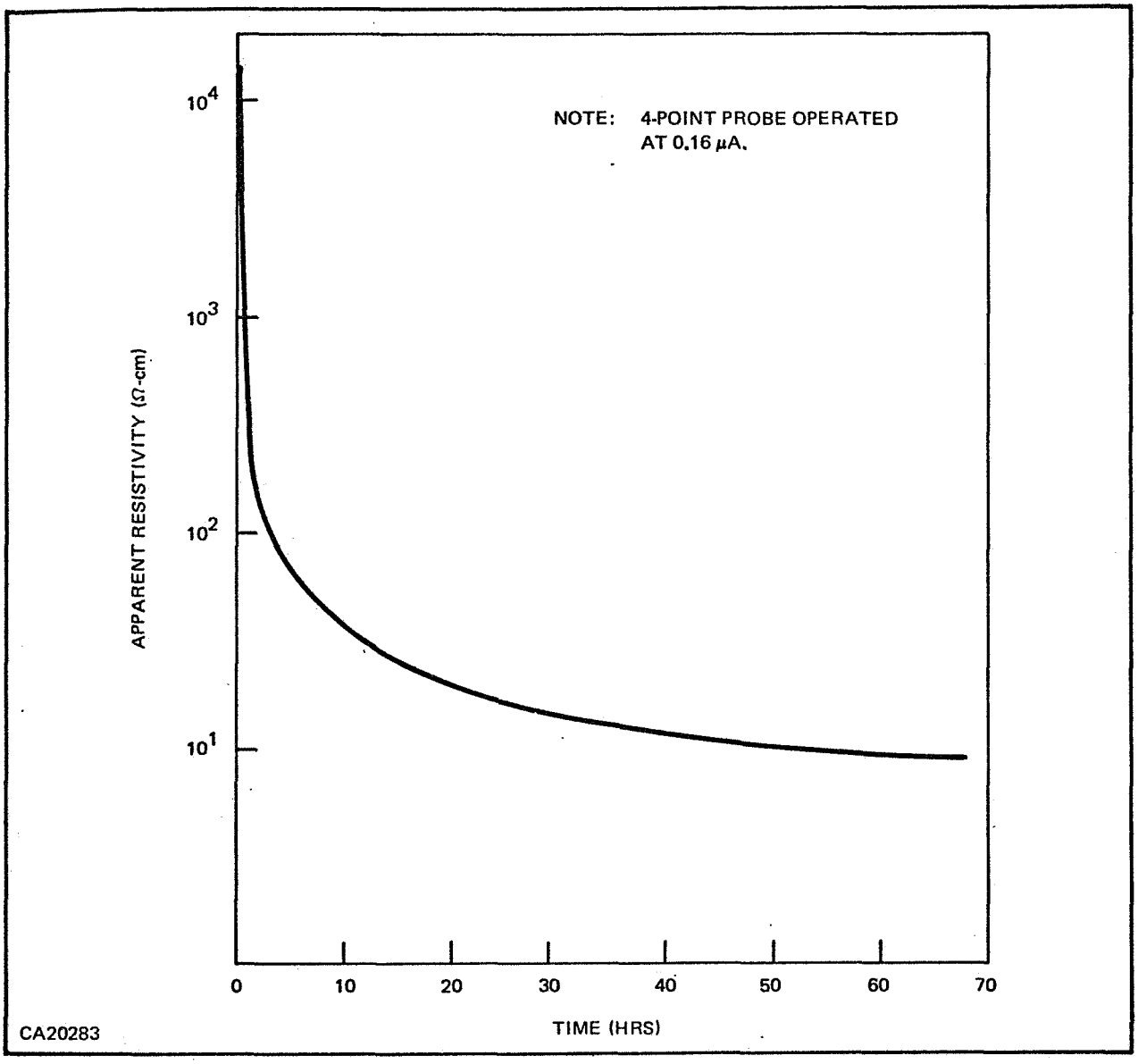

Figure 16. Apparent Resistivity of Li:B Compensated Sample for Extended Time

through the skin and not the bulk. Hall measurements on these samples reflect the behavior described, but the apparent carrier concentration and mobility are not meaningful in the absence of information on junction depth progression with time.

For a diffusion limited process, the apparent resistivity of Figures 15 and 16 should decrease as the square root of time, $t^{-1/2}$, at least if one assumes the mobility is approximately constant. However, when plotted as a log-log graph, it happens that the apparent ρ decreases as $t^{-3/2}$ over several orders of magnitude of ρ. After about 100 hours, however, the dependence finally becomes $t^{-1/2}$. Thus, the lithium diffuses out of the sample much too fast at first. This may be due to the large built-in fields that develop in the surface region when the lithium diffuses away from the boron very near the surface. For illustration, the diffusion zone [namely $(D_{Li}t)^{1/2}$] for lithium at

room temperature is about 100 Å after 10 minutes. This can be shown to give a built-in electric field of over 10^5 volts cm^{-1} in the out-diffused region. A more likely possibility is that the lapped surface is similar to a polycrystalline region, and the lithium is diffusing to regions similar to grain boundaries. Such a situation can lead to a $t^{-3/2}$ dependence*, [15].

E. LITHIUM COMPENSATED PHOSPHORUS-DOPED SILICON

The lithium species generally observed in silicon is an interstitial donor. However, from a thermodynamic standpoint there must also be some finite concentration of a substitutional lithium species which would be expected to be acceptor, defined as Li_{Si}^- when ionized. As an example of this type of behavior, Li in GaAs can be either an interstitial donor or a substitutional acceptor.[18] The donor form is dominant in heavily P-type GaAs and the acceptor form dominates in heavily N-type GaAs. The identification of Li_{Si}^- could be important to theoretical understanding of the annealing processes observed in silicon solar cells following electron irradiation.

To test for such a species in silicon, lithium was diffused into heavily N-type silicon (phosphorus doped) and observed the change in resistivity and electron mobility. The substitutional lithium concentration should be enhanced by the factor n/n_i, where n is the free electron concentration (which is essentially the phosphorus concentration) and n_i is the intrinsic electron concentration at the diffusion temperature. For a temperature of 1000°C, n_i is 8×10^{18} cm^{-3}, so for a phosphorus concentration of 5.4×10^{19} cm^{-3} the enhancement factor, n/n_i, is about 7. The interstitial donor form of lithium should be depressed by a similar factor. This simple treatment is not precise because of the high solubility of the lithium in otherwise undoped silicon. This is about 5×10^{19} cm^{-3} at 1000°C, which exceeds n_i and complicates the analysis somewhat. Nevertheless, the same principles apply, and we should be able to make some reasonable estimate of the lithium substitutional concentration at 1000°C from the observed change in carrier concentration in heavily phosphorus-doped silicon. Similar data at other diffusion temperatures should allow estimates to be made of the feasibility of the formation of substitutional lithium following an irradiation event, for example by the reaction:

$$Li_I^+ + V_{Si} \rightarrow Li_{Si}^- + 2e^+$$

The data for sequential lithium diffusions at 1000°C using the silicon enclosure are shown in Table III. The repeated diffusions were necessary to avoid depleting the lithium sources. This occurred by oxidation primarily and was made evident after about one hour of diffusion at 1000°C by the attendant decrease in the sample resistivity (after an initial increase).

The data in Table III show that the average resistivity increases by a factor of 2.7 and the effective mobility shows no significant change. If the latter had increased significantly, an ion-pairing mechanism between the lithium acceptors and phosphorus donors would have been indicated, since this would have reduced the concentration of ionized scattering centers. However, since it did not change, we must assume that the primary effect is the introduction of lithium substitutional acceptors, Li_{Si}^-. The concentration of acceptors added is about 3.5×10^{19} cm^{-3}.

Control runs on companion phosphorus-doped samples showed no change in resistivity on heating at 1000°C for periods of several hours.

* We are grateful to Dick Bass of Northrup Aviation Center for this suggestion.

Table III. Sample Resistivity, Mobility, and Carrier Concentration Versus Lithium Diffusion Time*

Cumulative Diffusion Time (min)	Resistivity (Ω-cm)	Carrier Concentration (cm^{-3})	Mobility ($cm^2 volt^{-1} sec^{-1}$)
0	1.68×10^{-3}	5.4×10^{19}	69
30	1.79×10^{-3}	5.4×10^{19}	66
65	1.94×10^{-3}	4.7×10^{19}	68
90	2.35×10^{-3}	3.9×10^{19}	69
120	3.05×10^{-3}	3.2×10^{19}	64
150	3.62×10^{-3}	3.0×10^{19}	64
270	4.49×10^{-3}	1.9×10^{19}	71

*Times include time for lithium to penetrate carrier slices (see Text and Figures 6 and 7).

From the estimate of the substitutional lithium concentration in heavily phosphorus-doped silicon, the solubility enhancement arguments can be reversed and the substitutional lithium concentration in silicon containing only lithium can be estimated to be about 1/7 of that in the phosphorus-doped case. Thus, the concentration of Li_{Si}^{-} in silicon doped only with lithium to its solubility limit at 1000°C is about 5×10^{18} cm^{-3}, which represents about 10% of the total lithium in the sample at this temperature. This confirms the view that lithium is primarily an interstitial donor ($\approx$ 90%), but suggests that a measurable substitutional concentration also exists, at least at 1000°C.

F. SOLAR CELL FABRICATION

1. Basic Fabrication Processes

The two basic fabrication processes used on the contract are outlined in the simplified flow diagram of Figure 17. The "standard" process (right sequence) used a pre-sized blank with the lithium applied by evaporation techniques through a "picture-frame" mask. This technique, while preventing Li overspray to the "p" active surface, resulted in non-uniform Li doping around the edges of the cell.

It is significant that Li was introduced by evaporation of elemental Li on all cells fabricated under this contract. The details of the Li evaporation techniques are as follows:

Source – high purity (< 0.005% Na) elemental Li wire, 2 charges 1 1/4 inch long X 1/8 inch diameter.

Source Preparation – rinsed in semiconductor grade acetone until all visual oxidation removed. Rinse performed immediately prior to system evacuation.

Source Loading – transferred from acetone rinse directly to source container at room temperature.

Source Container – tantalum boat, 2 X 0.5 X 0.015 inches resistant heated.

Substrate – boron diffused, N-type silicon.

Substrate Preparation – boron deglazed in semiconductor grade hydrofluoric acid 5 minutes, multiple rinses in flowing deionized water, acetone rinsed and dried in nitrogen ambient immediately prior to mask loading.

Substrate Loading – transferred to metal mask in pure-aire hood. Loaded mask transferred to vacuum system with substrate heaters set at 200°C.

Vacuum System – CVC model 18, 6 inch oil diffusion pump with freon refrigeration trapping.

System Geometry – center of substrate plate 6 inches above source boat. Infrared heaters directly above substrate plate. Thermocouple mounted to substrate plate for external temperature monitoring.

Source Deposition – system evacuated to a pressure of 5×10^{-5} mm Hg or less. Substrate stabilized at a temperature of 200 ± 10°C. Current to source boat slowly increased to initiate Li evaporation at a rate sufficiently low to minimize "sputtering" of Li. Deposition rate and temperature of source not monitored. Partial pressure of contaminants not monitored. Source evaporated to completion and power to source boat slowly returned to zero. System backfilled with nitrogen to atmospheric pressure.

Li Diffusion – substrate plate removed from vacuum system at 200°C and tranferred to pure-aire hood. Substrates removed from substrate plate (maintained at ≈ 100°C during transfer) and loaded in preheated quartz diffusion boat. Diffusion boat removed from Li furnace hot zone immediately prior to loading. Quartz boat transferred to diffusion furnace immediately after loading. Li diffusion performed in forming gas (90% N_2: 10% H_2) at time and temperature specified in succeeding section "Process Variables."

The "whole slice" process (left sequence) was designed to eliminate the edge problems encountered with the standard process. Lithium was evaporated on the whole slice with techniques identical to the standard process technique. Two cells were sawed from each whole slice after Ti-Ag contact evaporation and sintering.

Figure 18 is an actual photograph of the "p" contact surface of a whole slice prior to the sawing operation. The whole slice process yielded two 1 X 2 cm, 5-grid cells (active area = 1.8 cm^2); whereas, the standard process cells were 1 X 2 cm, 3-grid (active area = 1.9 cm^2). The Ti-Ag contact sintering operation for either process was identical, i.e., 600°C for 3 minutes in forming gas

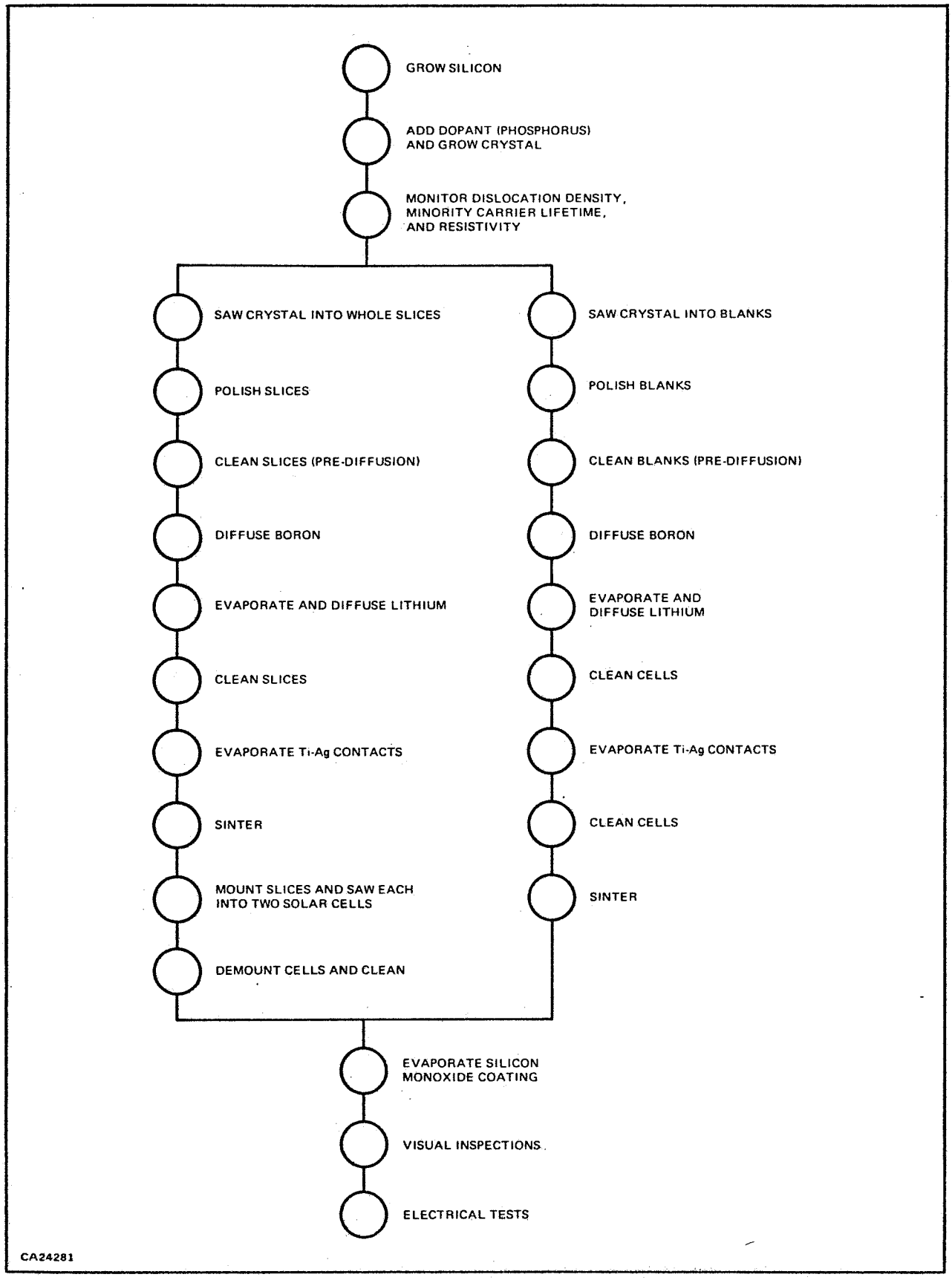

Figure 17. Lithium-Diffused Solar Cell Process Flow Diagram

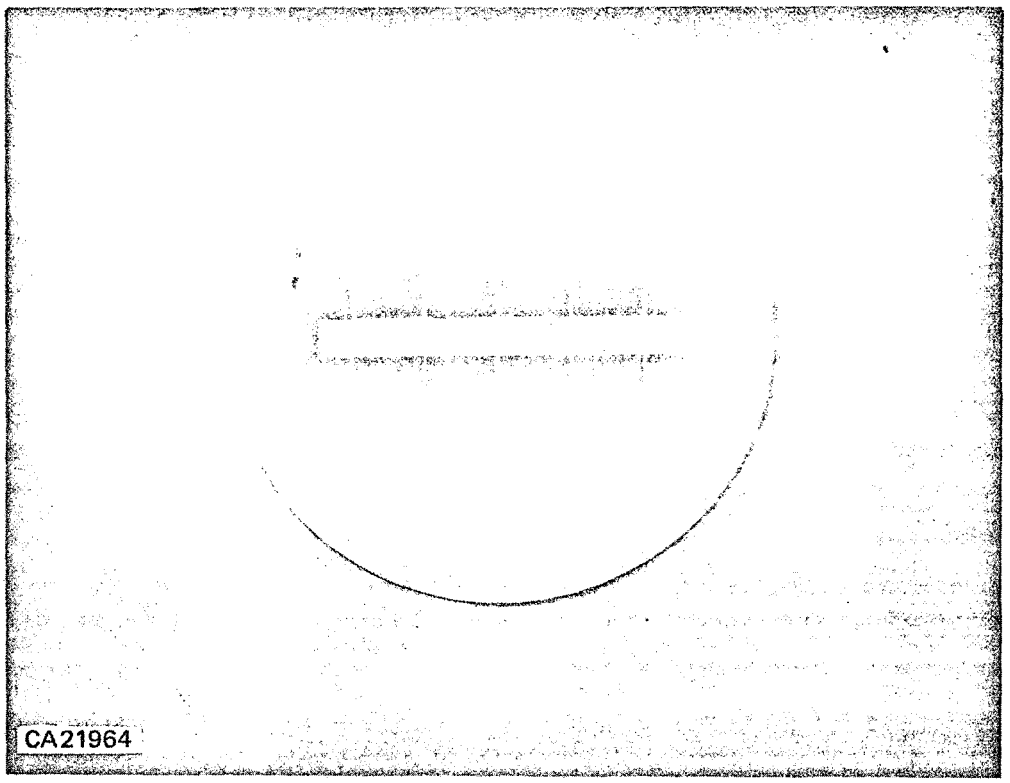

Figure 18. "P" Contact Surface of Whole Slice After Contact Deposition

ambient. All cells fabricated on the contract were nominally 0.013-inch thick with evaporated, quarter-wave silicon monoxide antireflective coatings.

2. Process Variables

Ten lots of lithium-diffused solar cells were supplied on the contract. Each lot contained 60 cells fabricated identically. The major variables on the lots were lithium concentration at the junction, lithium uniformity at the periphery of the cell and the basic silicon crystal processing (float-zoned, Czochralski and *Lopex*). The variables associated with each shipping lot are summarized in Table IV.

All starting silicon on the contract was phosphorus doped with the Czochralski resistivity being > 20 Ω-cm and the *Lopex* and float-zoned being > 50 Ω-cm. Note that only lot T-2 received an additional redistribution cycle of 120 minutes at 400°C after the primary lithium diffusion source was removed. However, all lots were sintered after contact deposition at 600°C for approximately 3 minutes, which is a significant redistribution cycle in itself – equivalent to one hour at 400°C. Further, on the basis of the arguments presented relative to Figure 13, redistribution should not be required and may even be detrimental to the radiation recovery properties.

The boron diffusion processes on lots T-1 through T-9 were identical to those used on the previous contract. The resultant boron profile is reproduced in Figure 19. The diffusion time on lot

Table IV. Shipping Lot Variables and Electrical Results

Lot No.	Material-Li Diffusion-Process			Average Output (100 mW/cm^{2}W)		
				I_{sc} (mA/cm^2)	V_{oc} (mV)	Eff. (%)
T-1	Czochralski	90 min at 400°C	Std	29.2	591	11.8
T-2	Czochralski	90 min at 400°C	Std†	30.1	564	11.3
T-3	*Lopex*	90 min at 400°C	Std	30.0	589	12.1
T-4	Float-Zoned	90 min at 400°C	Std	27.9	586	11.2
T-5	*Lopex*	90 min at 400°C	W.S.+	29.1	600	12.7
T-6	*Lopex*	8 hrs at 325°C	Std	31.0	596	12.2
T-7	Czochralski	8 hrs at 325°C	Std	30.6	588	11.8
T-8	Czochralski	8 hrs at 325°C	W.S.	31.1	589	12.6
T-9	*Lopex*	8 hrs at 325°C	W.S.	30.6	598	12.7
T-10	*Lopex*	135 min at 400°C	W.S.‡	30.3	597	12.7

†Std + 120 min redistribution at 400°C

+W.S. – whole slice process

‡ Boron diffusion depth twice standard depth

T-10 was modified to yield a junction depth, x_j, twice that of lots T-1 through T-9. Lots T-5, T-9 and T-10 are three *Lopex* lots with the lithium concentration at the junction on T-5 theoretically being twice that of T-9 and T-10 being even higher than that of T-5 due to the increased junction depth and lithium diffusion time. Post-irradiation testing on these three lots should resolve the relative importance of lithium concentration at the junction on recovery characteristics of *Lopex* cells.

A direct comparison of *Lopex* to Czochralski starting material can be obtained by comparing lots T-8 to T-9.

G. CELL ELECTRICAL TESTING

1. Output 100 mW/cm^2 Tungsten

Each cell shipped on the contract was tested under a tungsten light source at 100 mW/cm^2 sunlight equivalent intensity. The tungsten bulbs were operated at a color temperature of 2870°K. A 1/4 inch thick plate glass filter with 3 cm deionized water was placed between the bulbs and the solar cell under test. The intensity was calibrated with a N/P Table Mountain standardized solar cell. Data were taken at a cell active surface temperature of 28 ±2°C.

The average output of each shipping lot under the tungsten source is summarized in Table IV. The short-circuit current is presented on a mA/cm^2 basis for direct comparison. The whole slice process cells were 1.8 cm^2 active area whereas, the standard process cells were 1.9 cm^2. The conversion efficiency was calculated at the maximum power point on each cell.

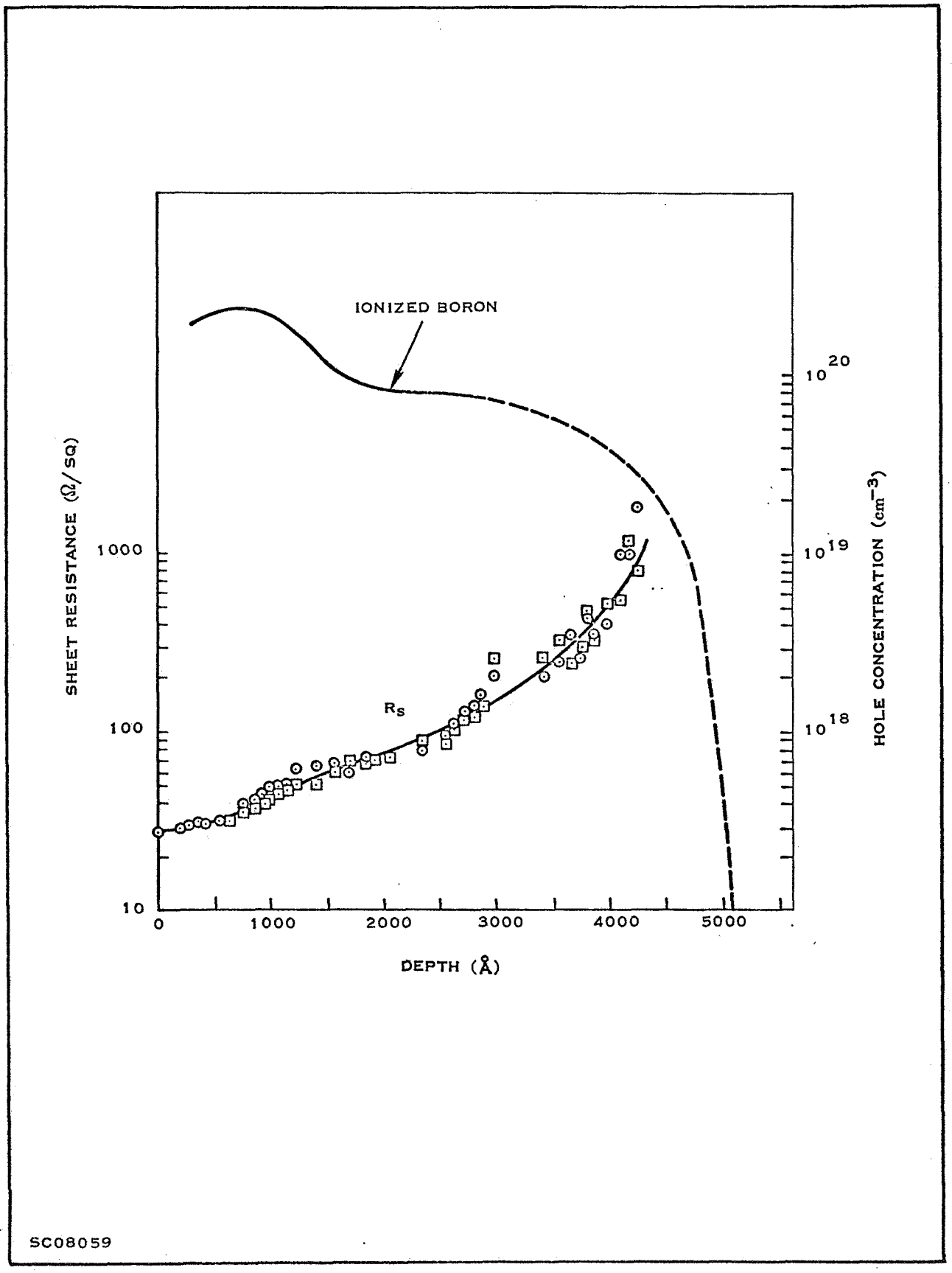

Figure 19. Boron Diffusion Profile Prior to Lithium Diffusion

The major variance in open-circuit voltage occurred on lot T-2, which received a 120 minute lithium redistribution cycle at 400°C after the prime lithium source was removed. This lot exhibited one of the lower efficiencies, 11.3%. The whole slice lots were extremely uniform in output characteristics when compared to the standard process lots, demonstrating the importance of uniform lithium doping across the entire solar cell. The standard process cells varied electrically to such a degree that it is difficult to draw specific conclusions concerning the affect of the major variable of the lot, i.e., base material or Li diffusion cycle. However, a comparison of whole slice lots T-8 and T-9 reveals the conversion efficiency of Czochralski and *Lopex* material to be virtually the same for the same lithium diffusion cycle. The outputs of the three *Lopex*-whole slice lots with three different lithium diffusion cycles were statistically identical. Post-irradiation annealing results of these lots should resolve the importance of the lithium diffusion cycle and resultant concentration profile.

Electrical data under the tungsten source of the 600 cells shipped on the contract is detailed in Appendix B.

2. Output 140 mW/cm^2 Filtered-Xenon

The output characteristics of lots T-6 and T-7 were measured under TI's AM0 filtered-xenon solar simulator, whose spectral irradiance is compared to Johnson's Curve in Figure 20.[19] Although the TI simulator curve deviates significantly from the Johnson curve, the total integrated result (considering a typical N/P spectral-response characteristic) would be 0.3 mA more short-circuit current output for a 1 X 2 cm, 3-grid cell under the TI simulator than under AM0 sunlight.

The simulator's intensity was established at 140 mW/cm^2 using a N/P working standard (traceable to a JPL balloon standard calibration). The active surface temperature of the cells under test was 28 ± 2°C. Individual cell readings are detailed in Tables V and VI for T-6 and T-7, respectively. The data on T-6 were taken at a load voltage of 0.485 V, instead of the conventional 0.430 V, to give a more accurate evaluation of the AM0 conversion efficiency. These 60 cells averaged 9.65% AM0 efficiency under the simulator. This lot was one of the higher efficiency standard process lots, averaging 12.2% under the 100 mW/cm^2 tungsten test set.

The whole slice lots consistently averaged higher conversion efficiencies than the standard process lots. Five typical cells from lot T-5 (whole slice process) averaged 10.46% AM0 under the simulator at a load voltage of 0.485 V.

3. Spectral Response

The spectral response of cells from shipping lot T-5 was determined to be virtually identical to a typical N/P solar cell. The intensity of the tungsten light source and the filtered-xenon simulator were calibrated with the same N/P standard cell and the output of five whole slice cells (T-5) were measured under both sources. T-5 was *Lopex* base material with a 90 minute at 400°C lithium diffusion cycle. The electrical data under the two light sources are presented in Table VII. The short-circuit current of the cells averaged 60.6 mA and 61.0 mA under the tungsten and xenon sources, respectively. This data shows that the lithium diffused cells, at least lot T-5, have spectral response characteristics very similar to N/P solar cells.

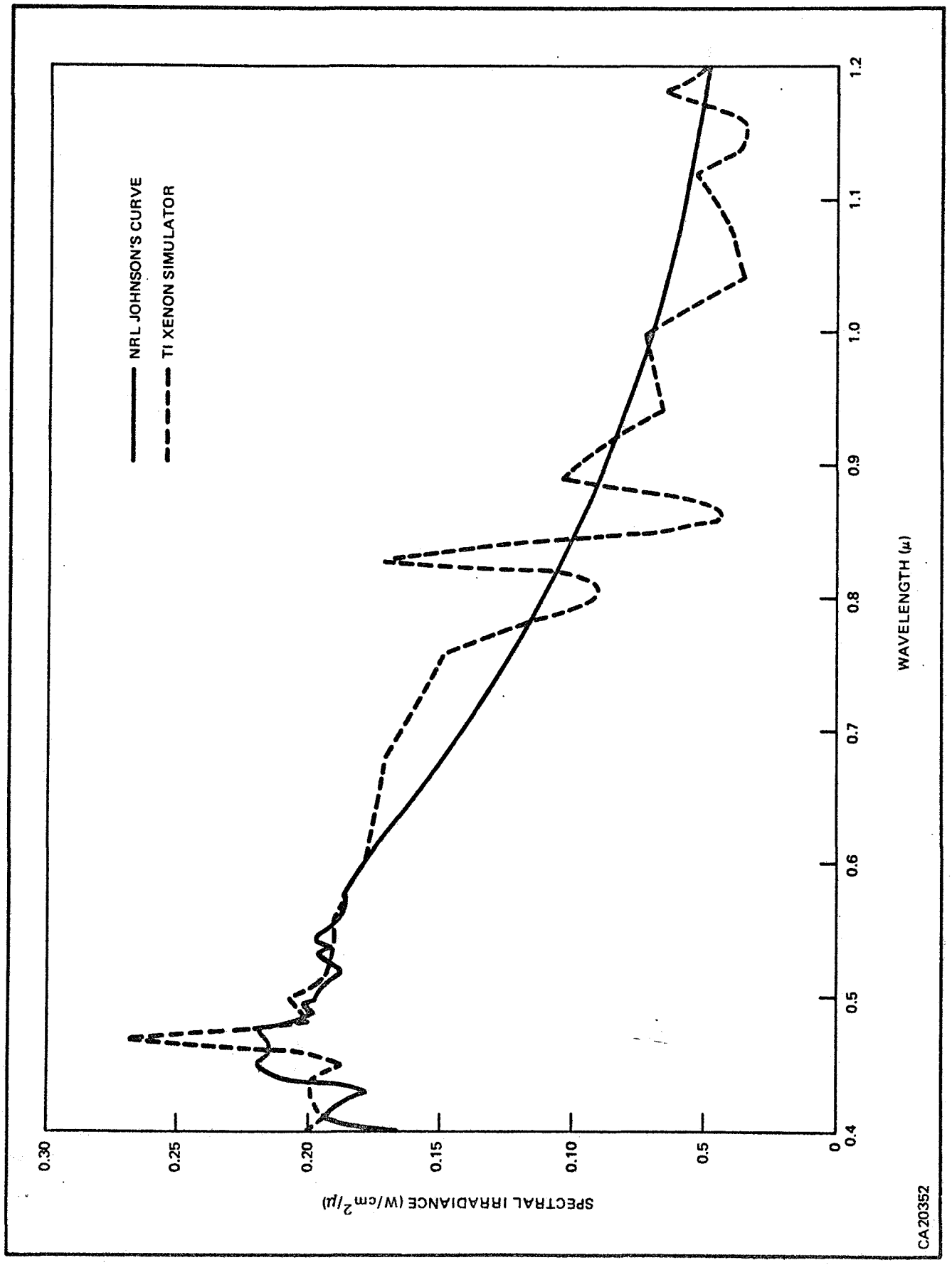

Figure 20. Comparison of Spectral Irradiance of TI Filtered-Xenon Simulator to Johnson Curve for AM0 Sunlight

Table V. Cell Characteristics of Lot 6 Under AM0 Simulator
(8-Hour Diffusion at 325°C on *Lopex* Silicon)

Cell No. T-6	I_{sc} (mA)	$I_{0.485}$ (mA)	V_{oc} (mV)	Cell No. T-6	I_{sc} (mA)	$I_{0.485}$ (mA)	V_{oc} (mV)
1	66.5	53.6	595.8	32	68.9	51.9	593.5
2	67.3	49.9	587.9	33	64.6	50.4	589.6
3	69.1	54.9	596.3	34	69.7	55.2	598.3
4	66.9	50.1	583.3	35	64.0	49.3	586.9
5	66.3	52.1	596.2	36	69.4	52.7	597.1
6	68.9	54.2	595.3	37	66.6	52.8	597.2
7	68.2	55.0	599.9	38	67.1	52.1	597.8
8	65.7	48.8	585.8	39	68.7	56.1	600.3
9	67.4	51.7	595.3	40	70.5	53.1	595.2
10	68.6	51.8	592.2	41	67.2	52.3	590.6
11	67.7	52.7	587.7	42	67.8	51.4	595.8
12	67.5	54.6	597.8	43	69.9	60.3	602.9
13	67.7	50.2	593.2	44	69.6	50.1	587.2
14	67.9	51.3	595.0	45	70.9	58.9	600.4
15	68.2	49.4	588.4	46	68.7	53.7	597.7
16	67.2	53.1	594.3	47	69.8	51.3	595.8
17	67.1	50.3	587.8	48	70.3	53.8	592.9
18	68.2	50.6	588.2	49	69.4	52.2	593.5
19	68.8	52.7	590.4	50	67.1	49.9	583.7
20	68.3	53.6	593.8	51	65.9	51.3	594.1
21	66.4	55.0	594.7	52	68.9	49.4	592.1
22	68.1	49.9	588.5	53	70.3	58.4	601.8
23	66.2	53.8	597.4	54	70.6	54.6	598.0
24	66.1	53.3	594.5	55	67.3	58.0	607.0
25	66.7	49.2	581.8	56	68.1	52.8	597.9
26	68.0	51.9	598.2	57	66.7	56.1	600.5
27	68.6	51.8	588.9	58	67.4	57.7	604.0
28	69.8	61.0	606.2	59	67.3	52.4	597.7
29	68.4	49.6	590.3	60	68.4	53.7	601.0
30	67.9	54.0	596.4				
31	70.7	54.9	596.2				
				Avg.	68.0	52.8	594.3

Table VI. Cell Characteristics of Lot 7 Under AM0 Simulator (8-Hour Diffusion at 325° C on Czochralski Silicon)

Cell No. T-7	I_{sc} (mA)	V_{oc} (mV)	$I_{0.430\ V}$ (mA)	Cell No. T-7	I_{sc} (mA)	V_{oc} (mV)	$I_{0.430\ V}$ (mA)
1	68.7	584.7	60.2	31	66.8	589.0	60.3
2	70.0	590.5	63.2	32	68.0	604.1	65.3
3	68.6	589.7	62.2	33	68.7	591.3	58.8
4	72.9	593.3	62.8	34	66.8	593.8	59.3
5	71.4	593.8	62.5	35	68.3	595.8	63.5
6	68.8	592.8	61.2	36	63.8	595.4	60.8
7	68.1	581.4	58.2	37	66.5	583.8	57.7
8	68.0	594.1	61.7	38	68.9	591.5	60.7
9	68.1	585.8	60.2	39	66.8	592.6	61.4
10	66.7	589.0	59.1	40	70.3	594.6	62.7
11	71.2	585.5	59.4	41	69.8	570.7	55.5
12	73.3	593.8	60.7	42	68.3	586.6	60.5
13	68.1	593.3	61.2	43	68.4	595.5	64.4
14	68.0	586.1	58.2	44	60.6	596.9	57.8
15	72.8	587.2	61.8	45	70.6	585.5	58.5
16	69.0	586.4	60.7	46	68.3	588.8	59.3
17	71.4	594.4	63.1	47	67.3	578.4	57.5
18	69.1	594.9	62.4	48	70.0	589.3	59.1
19	68.8	587.5	61.3	49	67.5	592.8	61.3
20	69.8	588.9	62.8	50	70.3	588.6	61.3
21	70.0	596.6	65.8	51	70.2	595.4	63.8
22	69.8	598.3	64.6	52	72.4	598.5	66.5
23	68.1	589.6	55.5	53	66.6	591.6	59.6
24	69.8	602.5	66.5	54	67.6	598.3	63.9
25	70.9	587.1	62.0	55	69.4	588.0	59.6
26	69.0	591.9	59.0	56	70.5	588.5	61.4
27	67.3	592.8	60.3	57	65.1	589.7	60.0
28	67.6	582.8	58.4	58	67.8	577.9	58.6
29	69.9	596.5	63.8	59	70.7	600.5	65.5
30	71.7	596.4	64.4	60	72.3	587.7	62.5
				Avg.	68.9	590.9	61.2

Table VII. Results of Solar Simulator and Tungsten Light Source Tests–Lot T-5

Cell Number	I_{sc} (mA)		V_{oc} (V)		$I_{0.485\ V}$ (mA)		Eff (%AM0)	
	W	Xe	W	Xe	W	Xe	W	Xe
1	58.4	59.1	601.3	601.8	53.2	53.7	10.21	10.31
2	59.7	60.2	599.3	600.0	52.9	53.5	10.17	10.27
3	61.4	62.1	602.0	602.9	54.7	54.9	10.50	10.54
4	61.8	62.1	603.3	603.7	55.9	56.1	10.73	10.77
5	61.8	61.6	603.6	603.3	54.4	54.1	10.44	10.39
$\bar{X}$	60.6	61.0	601.9	602.3	54.2	54.5	10.41	10.46

SECTION III

CONCLUSIONS

The major contributions of this report are listed.

1) Evaporated lithium diffused from the back to the front of a solar cell is an effective production process that results in a high efficiency solar cell comparable to standard N/P cell.

2) Lithium can be effectively diffused into silicon from the vapor phase in a "silicon enclosure," but the diffusion temperature must be over 525°C for diffusion in a furnace under dry nitrogen.

3) The lithium surface concentration can be reduced by using a lithium-tin alloy as a vapor source, but the oft-attendant oxidation of lithium makes it difficult to apply as a production process.

4) The electron mobility and minority carrier (hole) lifetime of lithium-diffused silicon is comparable to the very best n-type silicon doped with other donors such as arsenic or phosphorus.

5) Lithium can be used to closely compensate very heavily boron-doped silicon. The lithium very near the surface of this compensated silicon out-diffuses and causes the apparent resistivity by four-point probe to decrease with time. The time dependent apparent resistivity suggests that something like grain-boundary diffusion near the surface may be involved in the surface shunt that develops.

6) Although lithium in silicon is predominately an interstitial donor, the partial compensation of heavily phosphorus-doped silicon with lithium suggests that a measurable substitutional lithium acceptor solubility exists at 1000°C.

7) The whole slice fabrication process yields a high efficiency solar cell that has a uniform lithium and boron distribution across the whole cell.

8) Lithium diffusion times of 90 minutes at 400°C or 8 hours at 325°C, each with no additional "redistribution" cycle gave good results. The latter process yielded slightly higher efficiencies. This may be due to the lower average lithium concentration of these cells.

9) *Lopex* and Czochralski silicon yield lithium-diffused solar cells of virtually the same conversion efficiency when the whole slice process is used.

10) On the basis of the 60 cells in each of the ten lots, it should be possible to determine with reasonable certainty the importance of lithium concentration near the junction, and non-uniform lithium concentration near the edges of the cell. These are both expected to be important variables in initial efficiency, rate and extent of recovery after charged particle bombardment, and permanence of the recovery process (that is, the presence or absence of the so-called redegradation process).

SECTION IV

NEW TECHNOLOGY

The following items were reported to JPL on April 18, 1969 as new technology on contract 952248:

1) Substitutional Lithium.
   Innovator: Don Leslie Kendall
   Reference: Quarterly Report No. 2, p. 2
   Final Report, p. 14

2) Lithium Compensation of Boron-Doped Silicon.
   Innovator: Don Leslie Kendall
   Reference: Quarterly Report No. 2, p. 4
   Final Report, p. 23

SECTION V

REFERENCES

1. D. L. Kendall and R. A. Vineyard, Final Report under Contract No. NAS55-10274(Dallas, Texas: Texas Instruments Incorporated, 1968).

2. D. L. Kendall and D. De Vries, "Diffusion in Silicon," *Semiconductor Silicon,* ed. by R. R. Haberecht and E. L. Kern (Electrochemical Society: New York, 1969), pp. 358-421.

3. W. Shockley and J. L. Moll, *Phys. Rev.,* **119**, 1480 (1960).

4. F. A. Kroger, *The Chemistry of Imperfect Crystals,* (John Wiley & Sons: New York, 1964).

5. R. F. Peart, *Phys. Stat. Solidi,* **15**, K119 (1966).

6. B. J. Masters and J. M. Fairfield, *Appl. Phys. Letters,* 8, 280 (1966).

7. J. M. Fairfield and B. J. Masters, *J. Appl. Phys.,* 38, 3148 (1967).

8. R. N. Ghoshtagore, *Phys. Rev. Letters,* **16**, 890 (1966).

9. G. D. Watkins, *Proceedings of the 7th International Conference on the Physics of Semiconductors, Paris 1964,* Vol. III, P. Baruch, ed. (Academic Press: New York, 1965), pp. 97-113.

10. D. L. Kendall, Phd. Dissertation, Stanford 1965, p. 12.

11. R. N. Ghoshtagore, *Phys. Stat. Solidi,* **20**, K89 (1967).

12. H. Reiss and C. S. Fuller, *Trans. AIME, J. Metals,* **206**, 276 (1956).

13. D. L. Kendall and R. A. Vineyard, *Conference Record of Sixth Photovoltaics Specialists Conference,* 3, 166 (1967).

14. M. Hansen, *Constitution of Binary Alloys* (McGraw-Hill: New York; 2nd Edition, 1959), p. 904.

15. H. Reiss and C. S. Fuller, "Diffusion Processes in Germanium and Silicon," *Semiconductors,* ed. by N. B. Hannay(Reinhold Publishing Corporation: New York, 1959), p. 262.

16. F. J. Morin and J. P. Maita, *Phys. Rev.*, **96**, 28 (1954); N. B. Hannay, *Semiconductors,* (Reinhold: New York, 1959) pp. 35, 38, 39, 359.

17. R. L. Williams, C. D. Williams and N. J. Harvey, *IEEE Transactions Nuclear Science,* **13**, 53 (1966).

18. D. L. Kendall, *Semiconductors & Semimetals,* Eds. R. K. Willardson and A. C. Beer, Vol. 4, (Academic Press: New York, 1968), p. 234.

19. F. S. Johnson, "The Solar Constant," *J. of Meteorology,* Vol. II, (1956) 436.

APPENDIX A
TABLES AND REFERENCES

Table I. Group IIIA acceptor diffusion coefficients in silicon.

	Element	Ref.	D_o (cm^2/sec)	Q (eV)	$D_{1300°C}$ (cm^2/sec)	$D_{1100°C}$ (cm^2/sec)	C_o Range (cm^{-3})	Remarks
B	Fuller, et al.	(1b)	10.5	3.69	1.6×10^{-11}	3.0×10^{-13}	$1.0 \times 10^{21} - 1.0 \times 10^{22}$	ISR, CD, $\bar{D}$
	Kurtz, et al.	(2)	*1.4	3.51	7.8×10^{-12}	1.8×10^{-13}	$1.6 \times 10^{17} - 7.0 \times 10^{18}$	pn, Consistent with low conc. data in Ref. (10) and (13)
	Yamaguchi, et al.	(3)	17.1	3.68	2.7×10^{-11}	5.3×10^{-13}	$2.0 \times 10^{20} - 5.0 \times 10^{20}$	Modified ISR
	Williams	(4)	16.0	3.69	See Text+	See Text+	Approximately 10^{21}	pn, CD, $\bar{D}$
	Kato, et al.	(5)	2.02	3.52	1.1×10^{-11}	2.4×10^{-13}	---- - ----	ISR, Redistribution during oxidation
	Nagano, et al.	(6)	**106.0	4.25	2.5×10^{-12}	2.6×10^{-14}	$1.0 \times 10^{15} - 1.0 \times 10^{17}$	ISR, Diffusion from a sputtered solid source
	Other Data: References (7), (8), (9), (10), (11), (12), (13), and (14).							
	Other Observations: References (41), (42), (43), (44), (45), (46), (47), (48), (49), (50), and (51).							
Al	Goldstein	(15)	2800	3.9	8.8×10^{-10}	1.4×10^{-11}		pn, CD
	Fuller, et al.	(1b)	8.0	3.47	6.0×10^{-11}	1.5×10^{-12}	$1.0 \times 10^{16} - 4.0 \times 10^{17}$	pn, Consistant with data in Reference (18)
	Miller, et al.	(16)	4.8	3.36	8.1×10^{-11}	2.2×10^{-12}	$1.0 \times 10^{18} - 2.7 \times 10^{19}$	Capacitance method, CD
	Kao	(17)	0.5	3.0	1.2×10^{-10}	4.9×10^{-12}	$3.0 \times 10^{18} - 1.3 \times 10^{19}$	SR, CD
	Navon, et al.	(18)						D_o, Q very similar to Ref.(1b)
Ga	Fuller, et al.	(1b)	3.6	3.51	2.0×10^{-11}	4.7×10^{-13}	$1.4 \times 10^{19} - 2.1 \times 10^{20}$	pn, CD
	Kurtz, et al.	(19)	*225	4.12	1.4×10^{-11}	1.7×10^{-13}	$1.4 \times 10^{17} - 4.4 \times 10^{18}$	pn and ISR
	Other Data: References (20), (21)+, (22)+, (41).							
In	Fuller, et al.	(1b)	16.5	3.90	5.2×10^{-12}	8.0×10^{-14}	$2.8 \times 10^{17} - 6.7 \times 10^{19}$	pn, CD
	Millea	(23)						T, Data consistent with Ref. (1b)
Tl	Fuller, et al.	(1b)	16.5	3.90	5.2×10^{-12}	8.0×10^{-14}	$9.0 \times 10^{16} - 1.2 \times 10^{17}$	pn, CD

* Calculated
** Recalculated Value, Author's Value Incorrect
T Tracer Measurements
pn p-n Junction Depth Measurements
ISR Incremental Sheet Resistance
SR Sheet Resistance and Assumed Distribution
CD Concentration Dependence Not Taken Into Account
$\bar{D}$ (D-bar) Average D Typical of High Concentration
\+ See Text for Comment

Table II. Group VA donor diffusion coefficients in silicon.

	Elements	Ref.	D_o (cm^2/sec)	Q (eV)	$D_{1300°C}$ (cm^2/sec)	$D_{1100°C}$ (cm^2/sec)	C_o Range (cm^{-3})	Remarks
P	Howard	(24) (25)	1500	4.42	1.0×10^{-11}	8.9×10^{-14}	$\sim 10^{18} - 4 \times 10^{20}$	
	Fuller, et al.	(1b)	10.5	3.69	1.6×10^{-11}	3.0×10^{-13}	$6.0 \times 10^{20} - 5.0 \times 10^{22}$	ISR, CD, $\bar{D}$
	Mackintosh	(26)	*0.0032	2.6	1.5×10^{-11}	3.0×10^{-13}	$\sim 10^{20}$	SR and junction depth, N_B = 5×10^{14} cm^{-3} prediffusion results (erfc dist.)
	Mackintosh	(26)	*4.9	3.7	6.7×10^{-12}	1.3×10^{-13}	3×10^{18}	SR and junction depth, N_B = 5×10^{14} cm^{-3} diffusion results (Gaussion dist.)
	Maekawa	(27)	*2.73	*3.58	9.1×10^{-12}	2.0×10^{-13}	$2.2 \times 10^{18} - 7.5 \times 10^{18}$	ISR and T, Low conc. ISR only
	Other Data: References (8), (11), (21), (23) (28), (29), (30), (31), (32), (33), (34). Other Observations: References (42), (43), (44), (45), (46), (47), (48), (49), (50), (51), (52), (53), (54), (55), (56), (57), (58), (59).							
As	Fuller, et al.	(1b)	0.32	3.56	1.2×10^{-12}	2.7×10^{-14}	$5.8 \times 10^{17} - 4.5 \times 10^{18}$	pn, CD, $\bar{D}$
	Armstrong	(35)	68.6	4.23	1.9×10^{-12}	2.0×10^{-14}	$\sim 10^{17} - \sim 10^{19}$	SR, CD
	Raju, et al.	(36)	2.564	3.87	1.0×10^{-12}	1.6×10^{-14}	$7.0 \times 10^{17} - 7.0 \times 10^{18}$	SR
	Hsueh	(37)	83,000	5.20	1.8×10^{-12}	6.8×10^{-15}	$1.0 \times 10^{19} - 2.0 \times 10^{19}$	SR
	Other Data:		Reference (21)					
Sb	Fuller, et al.	(1b)	5.6	3.95	1.2×10^{-12}	1.8×10^{-14}	$1.4 \times 10^{18} - 9.2 \times 10^{21}$	pn, CD, $\bar{D}$
	Petrov, et al.	(38)	0.112	2.86	7.6×10^{-10}	3.6×10^{-12}		T
	Rohan, et al.	(39)	12.9	3.98	2.2×10^{-12}	3.2×10^{-14}	$1.9 \times 10^{19} - 5.0 \times 10^{19}$	T, Recalculation indicates C_o values may be low by ≈ density of Si.
	Other Data: References (7), (10), (23), (40).							
Bi	Fuller, et al.	(1b)	1030	4.64	1.4×10^{-12}	9.6×10^{-15}	$1.0 \times 10^{17} - 2.4 \times 10^{18}$	pn, CD, $\bar{D}$
	Pomerrenig	(40a)	896	4.12	5.5×10^{-11}	6.7×10^{-13}		pn

NOTE: For legend, refer to Table I.

Table III. Other impurity diffusion coefficients in silicon.

	Element	Ref.	D_o (cm^2/sec)	Q (eV)	$D_{1300°C}$ (cm^2/sec)	$D_{1100°C}$ (cm^2/sec)	Remarks
H	Van Wieringen, et al.	(60)	9.4×10^{-3}	0.48	2.7×10^{-4}	1.6×10^{-4}	Mass spectrometry.
	Ichimya	(61)	4.2×10^{-5}	0.56	6.7×10^{-7}	3.7×10^{-7}	T, evolution of gas.
He	Van Wieringen, et al.	(60)	0.11	1.26	1.0×10^{-5}	2.6×10^{-6}	Mass spectrometry.
	Luther, et al.	(62)	5.1×10^{-4}	0.58	7.0×10^{-6}	3.8×10^{-6}	Rate of evolution from B-doped crystal.
N	Panteleev, et al.	(63)		4.55			Based on entropy of formation of NI_3
O	Logan, et al.	(64)	135	3.5	8.1×10^{-10}	1.9×10^{-11}	pn, after 450°C heat treatment.
	Haas	(65)	0.21	2.44	3.2×10^{-9}	2.3×10^{-10}	Internal friction calculation.
	Corbett, et al.	(65a)	0.23	2.561	1.4×10^{-9}	9.1×10^{-11}	Comparison of annealing data with internal friction measurements
	Other Data: References (66), (67), (68), (65b), (65c).						
Li	Fuller, et al.	(69)	9.4×10^{-3}	0.79	2.8×10^{-5}	1.2×10^{-5}	pn
	Fuller, et al.	(70)	2.3×10^{-3}	0.66	1.8×10^{-5}	8.7×10^{-6}	Ion drift, mobility.
	Maita	(71)	2.3×10^{-3}	0.72	1.1×10^{-5}	5.2×10^{-6}	Low temp., Ion pairing, relaxation method.
	Shashkov, et al.	(72)	2.2×10^{-3}	0.70	1.3×10^{-5}	5.9×10^{-6}	pn
	Pell	(73) (74)	2.5×10^{-3}	0.655	2.0×10^{-5}	9.9×10^{-6}	Out diffusion at high temp. and ion drift at low temp.
	Pratt, et al.	(75)	2.65×10^{-3}	0.63	2.5×10^{-5}	1.3×10^{-5}	ISR
	Igras, et al.	(76)	1.3×10^{5}	1.13			Mechanical polish
			1.3×10^{4}	1.13	Surface Diffusion		Chemical polish
Na	Svob	(77)	1.65×10^{-3}	0.72	8.1×10^{-6}	3.8×10^{-6}	pn
K	Svob	(77)	1.1×10^{-3}	0.76	4.0×10^{-6}	1.8×10^{-6}	pn
C	Newman, et al.	(78)	0.33	2.92	1.4×10^{-1}	6.3×10^{-12}	T
	Newman, et al.	(78a)	1.9	3.1	2.2×10^{-1}	7.9×10^{-12}	Reanalyzed data fo Ref. (78).
Ge	Petrov	(79)	6.26×10^{5}	5.28	7.3×10^{-1}	2.6×10^{-14}	T, Ge powder.
Sn	Millea	(23)	*2.16×10^{5}	*5.3	1.1×10^{-12}	3.5×10^{-15}	T, enhanced in n-type, same in p-type.
	Yeh, et al.	(80)	32	4.25	7.6×10^{-13}	8.0×10^{-15}	T, enhanced in n-type, same in p-type.
S	Carlson, et al.	(81)	0.92	2.2	3.1×10^{-8}	7.7×10^{-9}	Resistivity and Hall measurements.
Cu	Boltaks, et al.	(82)	4×10^{-2}	1.0	2.5×10^{-5}	8.5×10^{-6}	T, I-S diff.
	Hall, et al.	(83)	4.7×10^{-3}	0.43	2.0×10^{-4}	1.2×10^{-4}	T, (Interstitial D).
	Other Data: References (84), (85).						
Ag	Boltaks, et al.	(86)	2.0×10^{-3}	1.60	1.5×10^{-8}	2.7×10^{-9}	T
Au	Struthers	(84) (87)	1.1×10^{-2}	1.12	2.8×10^{-5}	8.5×10^{-7}	T, I-S (unlimited vac. sources).
	Boltaks, et al.	(88)	1.15×10^{4}	3.11	1.2×10^{-6}	4.4×10^{-8}	T, vacancy limited I-S.
	Wilcox, et al.	(89)	2.44×10^{-4}	0.39	1.4×10^{-5}	9.0×10^{-6}	T, Interstitial $\overline{D}$.
		(89a)	2.75×10^{-3}	2.04	7.9×10^{-1}	3.9×10^{-11}	T, Substitutional $\overline{D}$.
	Collins, et al.	(90)	1.85×10^{-2}	1.32	1.1×10^{-6}	2.6×10^{-7}	MOS Capacitance, assumed erfc. dist
	Other Data: References (7), (91), (92), (93).						

NOTE: See Table I for legend.

Table III (continued)

	Element	Ref.	D_o (cm^2/sec)	Q (eV)	$D_{1300°C}$ (cm^2/sec)	$D_{1100°C}$ (cm^2/sec)	Remarks
Zn	Malkovich, et al.	(94)	0.1	1.4	3.2×10^{-6}	7.3×10^{-7}	Electric field dependence studies.
	Fuller, et al.	(95)					Found $10^{-6} < D < 10^{-7}$ from 900°C to 1360°C.
Mn	Carlson	(96)					T, $D > 2 \times 10^{-7}$ at 1200°C.
Fe	Struthers	(84)	6.2×10^{-3}	0.87	1.0×10^{-5}	4.0×10^{-6}	T
	Collins, et al.	(85)					T, Postulate I-S mechanism.
Ni	Yoshida, et al.	(97)	1.3×10^{-2}	1.4	4.2×10^{-7}	9.4×10^{-8}	Measured elect. active Ni. Apparent D by annealing. Interstitial $D \approx 10^{-4}$ to 10^{-5} 700 to 900°C.
	Bonzel	(98)	0.1	1.91	7.5×10^{-8}	9.7×10^{-9}	T, surface decrease method, apparent D.
	Other Data: References (99), (100), (101).						

NOTE: See Table I for legend.

1. A.Seeger and K. P. Chik, *Phys. Stat. Sol.*, 29, 455 (1968).

1a. A. Seeger and M. L. Swanson, "Vacancies and Diffusion Mechanisms in Diamond-Structure Semiconductors," *Lattice Defects in Semiconductors*, ed. by R. R. Hasiguti, (University of Tokyo Press: Tokyo, 1968), pp. 93-130.

1b. C. S. Fuller and J. A. Ditzenberger, *J. Appl. Phys.*, 27, 544 (1956).

2. A. D. Kurtz and R. Yee, *J. Appl. Phys*, 31, 303 (1960).

3. J. Yamaguchi, S. Horiuchi and K. Matsumura, *J. Phys. Soc. Japan*, 15, 1541 (1960).

4. E. L. Williams, *J. Electrochem. Soc.*, 108, 795 (1961).

5. T. Kato and Y. Nishi, *Japan. J. Appl. Phys.*, 3, 377 (1964).

6. K. Nagano, S. Iwauchi and T. Tanaka, *Japan. J. Appl. Phys.*, 7, 1361 (1968).

7. W. C. Dunlap, Jr., H. V. Bohn and H. P. Mahon, Jr., *Phys. Rev.*, 96, 822 (1954).

8. C. S. Fuller and J. A. Ditzenberger, *J. Appl. Phys.*, 25, 1439 (1954).

9. J. E. Cline and R. G. Seed, *J. Electrochem. Soc.*, 105, 700 (1958).

10. Ohio State University Research Foundation, *The Dependence of the Diffusivities of Impurities in Silicon on Background Doping and Surface Concentration*, O. Thurston and J. Tsai, R. F. Rep. No. 1233-4 Q, Contract DA-36-039-SC-87426 (Columbus, Ohio), February 1962.

11. P. A. Iles and B. Leibenhaut, *Solid State Electronics*, 5, 331 (1962).

12. D. N. Mikhailova, *Soviet Phys.-Solid State*, 4, 2195 (1963).

13. S. Maekawa and T. Oshida, *J. Phys. Soc. Japan*, 19, 253 (1964).

14. M. Y. Ben-Sira and S. Bukshpan, *Solid State Communications*, 3, 15 (1965).

15. B. Goldstein, *Bull. Am. Phys. Soc., Ser. II*, 1, 145 (1956).

16. R. C. Miller and A. Savage, *J. Appl. Phys.*, 27, 1430 (1956).

17. Y. C. Kao, *Electrochem. Techn.*, 5, 90 (1967).

18. D. Navon and V. Chernyshov, *J. Appl. Phys.*, 28, 823 (1957).

19. A. D. Kurtz and C. L. Gravel, *J. Appl. Phys.*, **29**, 1456 (1958).

19a. B. I. Boltaks and T. D. Dzhafarov, *Soviet Phys.-Solid State*, **5**, 2649 (1963).

20. J. G. Kren, B. J. Masters and E. S. Wajda, *Appl. Phys. Letters*, **5**, 49 (1964).

21. M. Okamura, *Japan. J. Appl. Phys.*, **7**, 1067 (1968).

22. J. Okamura, *Japan. J. Appl. Phys.*, **7**, 1231 (1968).

23. M. F. Millea, *J. Phys. Chem. Solids*, **27**, 315 (1966).

24. B. T. Howard, Fall Meeting, Electrochemical Society, October 1957.

25. H. Reiss and C. S. Fuller, "Diffusion Processes in Germanium and Silicon," *Semiconductors*, ed. by N. B. Hannay (Reinhold Publishing Corporation: New York, 1959), p. 244.

26. I. M. Mackintosh, *J. Electrochem. Soc.*, **109**, 392 (1962).

27. S. Maekawa, *J. Phys. Soc. Japan*, **17**, 1592 (1962).

28. M. J. Coupland, *Proc. Phys. Soc. (London)*, **73**, 577 (1959).

29. J. L. Hartke, *J. Appl. Phys.*, **30**, 1469 (1959).

30. E. Tannenbaum, *Solid State Electronics*, **2**, 123 (1961).

31. V. K. Subashiev, A. P. Landsman and A. A. Kukharskii, *Soviet Phys.-Solid State*, **2**, 2406 (1961).

32. A. G. Nassibian and G. Whiting, *Solid State Electronics*, **8**, 843 (1965).

33. R. A. McDonald, G. G. Ehlenberger and T. R. Huffman, *Solid State Electronics*, **9**, 807 (1965).

34. M. L. Joshi and S. Dash, *IBM J. Res. Dev.*, **10**, 446 (1966).

35. W. J. Armstrong, *J. Electrochem. Soc.*, **109**, 1065 (1962).

36. P. S. Raju, N. R. K. Rao and E. V. K. Rao, *Indian J. Pure Appl. Phys.*, **2**, 353 (1964).

37. Y. W. Hsueh, *Electrochem. Techn.*, **6**, 361 (1968).

38. D. A. Petrov, J. M. Schaschkow and A. S. Belanovski, "Die Diffusion der Beimengungen im Silizium," *Semiconductors and Phosphors*, ed. by M. Shon and H. Welker, (Interscience Publishers, Inc.: New York, 1958), pp. 652-655.

39. J. J. Rohan, N. E. Pickering and J. Kennedy, *J. Electrochem. Soc.*, **106**, 705 (1959).

40. P. V. Pavlov, V. A. Pavlov, V. A. Panteleev and A. V. Maiorov, *Soviet Phys.-Solid State*, **6**, 305 (1964).

40a. D. Pomerrenig, *Acta. Phys. Austriaca*, **20**, 338 (1965).

41. A. S. Grove, O. Leistiko, Jr., and C. T. Sah, *J. Appl. Phys.*, **35**, 2695 (1964).

42. K. H. Nicholas, *Solid State Electronics*, **9**, 35 (1966).

43. R. Gereth, P. G. G. van Loon and V. Williams, *J. Electrochem. Soc.*, **112**, 323 (1965).

44. R. Gereth and G. H. Schwuttke, *Appl. Phys. Letters*, **8**, 55 (1966).

45. J. E. Lawrence, *J. Electrochem. Soc.*, **113**, 819 (1966).

46. E. Levine, J. Washburn and G. Thomas, *J. Appl. Phys.*, **38**, 81 (1967).

47. E. Levine, J. Washburn and G. Thomas, *J. Appl. Phys.*, **38**, 87 (1967).

48. T. L. Parker, *J. Appl. Phys.*, **38**, 3471 (1967).

49. J. E. Lawrence, *J. Electrochem. Soc.*, **115**, 860 (1968).

50. A. F. W. Willoughby, *J. Materials Sci.*, **3**, 89 (1968).

51. T. H. Yeh and M. L. Joshi, *J. Electrochem. Soc.*, **116**, 73 (1969).

52. R. B. Allen, H. Bernstein and A. D. Kurtz, *J. Appl. Phys.*, **31**, 332 (1960).

53. B. I. Boltaks and N. N. Matveeva, *Soviet Phys.-Solid State*, **4**, 444 (1962).

54. I. M. Sulkhodreva, *Soviet Phys.-Solid State*, **6**, 311 (1964).

55. Y. Sato and H. Arata, *Japan. J. Appl. Phys.*, **3**, 511 (1964).

56. E. Kooi, *J. Electrochem. Soc.*, **111**, 1383 (1964).

57. M. L. Joshi and F. Wilhelm, *J. Electrochem. Soc.*, **112**, 185 (1965).

58. T. J. Parker, *J. Appl. Phys.*, **38**, 3475 (1967).

59. M. C. Duffy, F. Barson, J. M. Fairfield, and G. H. Schwuttke, *J. Electrochem. Soc.*, **115**, 84 (1968).

60. A.Van Wieringen and N. Warmolitz, *Physica*, 22, 849 (1956).

61. T. Ichimiya and Furuichi, *International J. Appl. Radiation Isotopes*, 19, 573 (1968).

62. L. C. Luther and W. J. Moore, *J. Chem. Phys.*, 41, 1018 (1964).

63. V. A. Panteleev and E. I. Akinkina, *Zh. Fiz. Khim.*, 42, 922 (1968).

64. R. A. Logan and A. S. Peters, *J. Appl. Phys.*, 30, 1627 (1959).

65. C. Haas, *J. Phys. Chem. Solids*, 15, 108 (1960).

65a. J. W. Corbett, R. S. McDonald and G. D. Watkins, *J. Phys. Chem. Solids*, 25, 873 (1964).

65b. P. D. Southgate, *Proc. Roy. Soc. (London)*, B70, 800 (1957).

65c. P. D. Southgate, *Phys. Rev.*, 110, 855 (1958).

66. W. Kaiser and P. H. Keck, *J. Appl. Phys.*, 28, 822 (1957).

67. W. Kaiser, H. L. Frisch and H. Reiss, *Phys. Rev.*, 112, 1546 (1958).

68. R. A. Logan and A. S. Peters, *J. Appl. Phys.*, 28, 819 (1957).

69. C. S. Fuller and J. A. Ditzenberger, *Phys. Rev.*, 91, 193 (1953).

70. C. S. Fuller and J. C. Severiens, *Phys. Rev.*, 96, 21 (1954).

71. J. P. Maita, *J. Phys. Chem. Solids*, 4, 1546 (1958).

72. M. Shashkov and I. P. Akimchenko, *Soviet Phys.-Doklady*, 4, 1115 (1959).

73. E. M. Pell, *Phys. Rev.*, 119, 1014 (1960).

74. E. M. Pell, *Phys. Rev.*, 119, 1222 (1960).

75. B. Pratt and F. Friedman, *J. Appl. Phys.*, 37, 1893 (1966).

76. E. Igras and J. Waminski, *Phys. Stat. Sol.*, 20, K5 (1967).

77. L. Svob, *Solid State Electronics*, 10, 991 (1967).

78. R. C. Newman and J. Wakefield, *J. Phys. Chem. Solids*, 19, 230 (1961).

78a. R. C. Newman and J. Wakefield, "Diffusion and Precipitation of Carbon in Silicon," *Metallurgy of Semiconductor Materials,* Vol. 15, ed. by J. B. Schroeder, (Interscience Publishers: New York, 1962), pp. 201-208.

79. D. A. Petrov, Yu. M. Shashkov, and I. P. Akimchenko, *Voprosy Met. i. Fiz. Poluprovoduikov (Moscow, Akad. Nauk SSSR),* 130, Sbornik, 1957 (*Chem. Abst.* 54, 1960, p. 17190c.).

80. T. H. Yeh, S. M. Hu and R. H. Kastl, *J. Appl. Phys,* 39, 4266 (1968).

81. R. O. Carlson and E. M. Pell, *J. Phys. Chem. Solids,* 8, 81 (1959).

82. B. I. Boltaks and I. I. Sosinov, *Zh. Tekh. Fiz.,* 28, 679 (1958).

83. R. N. Hall, and J. H. Racette, *J. Appl. Phys.,* 35, 379 (1964).

84. J. D. Struthers, *J. Appl. Phys.,* 27, 1560 (1956).

85. C. B. Collins and R. O. Carlson, *Phys. Rev.,* 108, 1409 (1957).

86. B. I. Boltaks and H. Shih-yin, *Soviet Phys.-Solid State,* 2, 2283 (1961).

87. J. D. Struthers, *J. Appl. Phys.,* 28, 516 (1957).

88. B. I. Boltaks, G. S. Kulikov and R. Sh. Malkovich, *Soviet Phys.-Solid State,* 2, 2134 (1961).

89. W. R. Wilcox and T. J. La Chappelle, *J. Appl. Phys.,* 35, 240 (1964).

89a. W. R. Wilcox, T. J. La Chappelle, and D. H. Forbes, *J. Electrochem. Soc.,* 111, 1377 (1964).

90. D. R. Collins, D. K. Schroder and C. T. Sah, *Appl. Phys. Letters,* 8, 323 (1966).

91. G. J. Sprokel, *J. Electrochem. Soc.,* 112, 807 (1965).

92. F. H. Shaklee, J. B. Larkin and D. L. Kendall, to be published in *Proc. IEEE,* (Sept. 1969).

93. W. M. Bullis, *Solid State Electronics,* 9, 143 (1966).

94. R. Sh. Malkovich and N. A. Alimbarashvili, *Soviet Phys.-Solid State,* 4, 1725 (1963).

95. C. S. Fuller and F. J. Morin, *Phys. Rev.,* 105, 379 (1957).

96. R. O. Carlson, *Phys. Rev.,* 104, 937 (1956).

97. M. Yoshida and K. Saito, *Japan. J. Appl. Phys.,* 6, 573 (1967).

98. H. P. Bonzel, *Phys. Stat. Sol.* 20, 493 (1967).

99. J. H. Aalberts and M. L. Verheyke, *Appl. Phys. Letters* 1, 19 (1962).

100. Y. Tokumaru, *Japanese J. Appl. Phys.* 2, 542 (1963).

101. M. Yoshida and K. Furusho, *Japanese J. Appl. Phys.* 3, 541 (1964).

APPENDIX B
TABLES

Table I. Cell Characteristics of Lot T-1 Under 100 mW/cm^2 Tungsten Light

90 Minute Diffusion at 100°C into Silicon							
Cell No. T-1	I_{sc} (mA)	V_{oc} (mV)	E_{ff} (%)	Cell No. T-1	I_{sc} (mA)	V_{oc} (mV)	E_{ff} (%)
1B	58.0	600	13.0	31B	56.5	589	11.2
2B	57.5	600	12.5	32B	54.5	590	11.2
3B	55.8	600	12.8	33B	56.2	589	11.1
4B	56.5	600	12.5	34B	55.2	590	11.5
5B	56.5	600	12.8	36	59.8	590	12.2
6B	56.5	605	12.6	37	59.1	600	13.0
7B	57.5	596	12.2	38	57.0	590	11.6
8B	58.0	590	12.3	39	57.4	588	12.2
9B	57.2	592	12.2	40	56.2	590	12.0
10B	55.2	605	13.0	41	56.0	590	12.1
11B	57.0	590	12.0	42	53.6	590	11.7
12B	56.6	596	11.8	43	57.8	592	12.7
13B	56.2	595	11.8	44	55.5	589	11.5
14B	55.2	594	11.9	45	56.0	590	12.5
15B	55.0	595	12.0	46	57.2	582	11.2
16B	55.1	598	12.2	47	55.0	580	11.1
17B	54.5	600	12.2	48	54.0	585	11.5
18B	54.5	600	12.2	49	53.8	585	11.5
19B	55.1	585	11.2	50	54.2	589	11.8
20B	53.8	578	10.2	51	55.5	589	12.2
21B	54.8	582	10.5	52	54.0	592	12.1
22B	56.2	590	10.8	53	54.0	600	12.0
23B	57.5	590	12.1	54	54.0	585	11.6
24B	55.0	585	10.8	55	54.0	599	12.3
25B	57.2	588	11.2	56	53.8	590	12.1
26B	55.3	590	11.2	57	53.5	585	12.2
27B	54.4	588	11.0	58	53.8	592	11.4
28B	53.8	589	11.1	59	53.9	592	11.2
29B	55.0	580	10.7	60	52.8	590	11.2
30B	55.0	585	11.0	61	53.0	590	11.3
				Avg.	55.6	591	11.8

Table II. Cell Characteristics of Lot T-2 Under 100 mW/cm^2 Tungsten Light

90 Minute Diffusion at 400°C Followed By 2 Hour Redistribution at 400°C into Czochralski Silicon							
Cell No. T-2	I_{sc} (mA)	V_{oc} (mV)	E_{ff} (%)	Cell No. T-2	I_{sc} (mA)	V_{oc} (mV)	E_{ff} (%)
1	59.1	580	12.1	31	58.6	573	11.5
2	58.3	575	11.6	32	57.5	580	11.4
3	58.3	580	11.9	33	56.2	573	10.9
4	57.0	578	11.6	34	54.2	580	11.1
5	58.2	579	12.0	36	56.8	572	11.1
6	58.0	580	11.9	37	57.0	570	11.1
7	56.6	582	11.9	38	59.0	562	11.2
8	56.8	578	11.7	39	58.1	574	11.2
9	58.0	575	11.8	40	57.7	578	11.2
10	59.3	576	11.8	41	55.2	570	10.5
11	57.8	576	11.7	42	57.0	570	11.2
12	57.8	574	11.8	43	59.3	570	10.6
13	59.0	572	11.8	44	56.8	570	11.4
14	58.2	580	11.8	45	55.0	565	11.0
15	59.2	572	11.9	46	58.5	578	11.1
16	57.0	579	11.7	47	57.0	570	11.0
17	56.5	578	11.5	48	57.2	578	11.5
18	58.5	570	11.5	49	56.0	565	10.9
19	57.0	570	10.8	50	56.9	573	10.8
20	56.2	580	11.7	51	55.5	570	10.8
21	57.0	570	11.7	52	57.0	562	10.8
22	56.1	584	11.8	53	57.0	575	10.8
23	56.8	572	11.7	54	56.5	558	10.5
24	56.0	570	10.9	55	54.9	564	10.6
25	57.8	574	11.5	56	55.9	558	10.6
26	56.8	578	11.4	57	59.0	582	10.7
27	55.0	570	11.2	58	58.9	575	11.5
28	56.2	578	11.3	59	54.8	570	10.6
29	58.0	570	11.4	60	56.2	575	10.8
30	57.9	568	11.2	61	57.2	578	11.2
				Avg.	57.2	564	11.3

Table III. Cell Characteristics of Lot T-3 Under 100 mW/cm^2 Tungsten Light

90 Minute Diffusion at 400°C into *Lopex* Silicon							
Cell No. T-3	I_{sc} (mA)	V_{oc} (mV)	E_{ff} (%)	Cell No. T-3	I_{sc} (mA)	V_{oc} (mV)	E_{ff} (%)
1	58.2	595	12.8	31	56.5	580	11.4
2	56.8	590	12.2	32	57.8	590	11.3
3	57.8	592	12.6	33	55.5	590	11.6
4	57.0	590	12.2	34	56.9	590	12.1
5	56.8	595	12.6	35	54.8	588	11.6
6	57.0	590	12.5	36	56.5	578	11.1
7	57.2	590	12.2	37	58.1	595	13.1
8	56.0	595	12.6	38	59.5	595	13.0
9	55.8	592	12.1	39	58.5	600	13.2
10	57.3	585	12.1	40	59.0	598	13.0
11	57.9	588	12.1	41	58.8	590	12.5
12	56.5	590	12.1	42	58.2	599	12.8
13	56.5	593	12.2	43	58.5	599	12.9
14	56.8	592	12.5	44	59.2	590	12.5
15	57.0	574	11.8	45	58.8	590	12.2
16	56.0	590	11.8	46	58.5	590	12.2
17	56.1	590	12.1	47	58.0	590	12.1
18	56.8	588	11.7	48	58.9	590	12.3
19	57.8	580	11.8	49	59.6	590	12.1
20	58.3	580	11.8	50	57.5	590	12.0
21	57.2	580	11.8	51	58.6	590	12.1
22	55.0	592	11.9	52	58.5	578	11.4
23	56.0	588	11.5	53	57.5	585	11.7
24	54.5	588	11.5	54	59.0	585	11.9
25	57.0	572	11.1	55	57.0	590	12.5
26	55.1	590	11.5	56	57.5	593	12.5
27	54.5	589	11.4	57	56.5	590	12.1
28	57.0	582	11.5	58	55.0	595	12.2
29	53.5	580	11.4	59	56.0	590	12.0
30	57.8	589	11.8	60	57.5	590	11.9
				Avg.	57.1	589	12.1

Table IV. Cell Characteristics of Lot T-4 Under 100 mW/cm^2 Tungsten Light

90 Minute Diffusion at 400°C into Float-zoned Silicon							
Cell No. T-4	I_{sc} (mA)	V_{oc} (mV)	E_{ff} (%)	Cell No. T-4	I_{sc} (mA)	V_{oc} (mV)	E_{ff} (%)
1	53.9	590	12.0	31	52.6	590	11.1
2	54.2	591	12.0	32	52.7	590	11.0
3	55.6	583	11.6	33	53.7	585	11.2
4	53.0	587	11.5	34	53.0	582	11.0
5	54.0	587	11.1	35	53.8	588	11.5
6	53.5	589	11.6	36	53.7	582	11.0
7	54.0	585	11.5	37	51.8	588	11.2
8	54.0	590	11.5	38	53.8	590	11.1
9	54.0	590	11.6	39	52.9	582	11.1
10	55.0	588	11.4	40	53.0	580	11.0
11	52.0	590	11.6	41	53.2	582	11.0
12	52.6	590	11.5	42	52.0	580	10.9
13	52.0	589	11.6	43	52.1	588	11.2
14	53.0	584	11.5	44	54.0	588	11.2
15	52.8	590	11.6	45	53.6	580	11.0
16	53.0	589	11.5	46	52.0	590	11.2
17	54.0	585	11.4	47	52.2	590	11.1
18	52.3	590	11.2	48	52.0	590	10.8
19	52.5	588	11.2	49	52.5	582	10.9
20	54.0	583	11.2	50	51.8	588	10.9
21	54.6	582	11.2	51	52.5	580	10.5
22	54.0	585	11.3	52	52.0	580	10.9
23	53.2	588	11.2	53	51.8	582	11.0
24	53.8	590	11.1	54	50.0	590	11.0
25	53.2	585	11.3	55	51.9	587	10.9
26	52.5	590	11.5	56	52.8	580	10.9
27	51.7	590	11.3	57	53.0	580	10.7
28	52.0	585	10.8	58	54.8	588	10.9
29	52.1	585	10.9	59	53.0	585	10.9
30	53.0	580	11.1	60	52.8	582	10.9
				Avg.	53.0	586	11.2

Table V. Cell Characteristics of Lot T-5 Under 100 mW/cm^2 Tungsten Light

90 Minute Diffusion at 400°C into Whole Slice of *Lopex* Silicon							
Cell No. T-5	I_{sc} (mA)	V_{oc} (mV)	E_{ff} (%)	Cell No. T-5	I_{sc} (mA)	V_{oc} (mV)	E_{ff} (%)
1	53.0	595	12.2	31	52.8	605	13.1
2	53.0	600	12.8	32	53.0	604	13.1
3	52.0	605	12.8	33	52.0	599	12.1
4	51.0	606	12.8	34	52.0	600	12.6
5	54.0	600	13.1	35	51.2	599	12.3
6	52.2	601	12.9	36	51.0	600	12.6
7	52.0	610	13.0	37	53.0	600	12.3
8	52.9	606	13.0	38	52.0	600	12.5
9	53.2	600	12.9	39	52.0	602	12.9
10	54.0	606	13.6	40	51.5	600	12.6
11	55.0	600	12.8	41	53.0	600	12.7
12	52.1	600	12.9	42	52.8	600	12.7
13	52.9	600	12.9	43	52.2	609	13.6
14	52.4	600	12.3	44	53.8	600	13.0
15	51.0	605	12.7	45	54.5	590	12.3
16	52.8	610	13.2	46	51.4	600	12.8
17	53.0	595	12.5	47	53.9	595	12.8
18	54.5	600	12.9	48	56.5	602	13.8
19	52.8	605	12.9	49	52.5	600	12.8
20	51.0	600	12.2	50	51.8	600	12.1
21	51.5	605	13.2	51	52.5	600	12.8
22	51.8	605	12.8	52	51.2	596	11.9
23	51.8	600	12.6	53	50.0	599	12.3
24	51.0	610	12.8	54	51.5	600	12.1
25	52.0	600	12.5	55	50.0	595	11.5
26	51.0	605	12.8	56	51.0	595	12.0
27	51.0	600	12.6	57	52.2	595	11.8
28	53.5	605	13.1	58	50.5	600	12.2
29	52.0	600	12.8	59	50.0	601	12.5
30	54.0	602	12.5	60	52.8	591	11.8
				Avg.	52.3	600	12.7

Table VI. Cell Characteristics of Lot T-6 Under 100 mW/cm^2 Tungsten Light

8 Hour Diffusion at 325°C on *Lopex* Silicon							
Cell No. T-6	I_{sc} (mA)	V_{oc} (mV)	E_{ff} (%)	Cell No. T-6	I_{sc} (mA)	V_{oc} (mV)	E_{ff} (%)
1	59.0	599	12.5	31	61.0	599	12.8
2	58.5	590	11.9	32	59.0	600	12.2
3	60.2	599	12.6	33	57.0	592	11.8
4	58.0	595	11.8	34	59.0	600	12.3
5	59.0	599	12.2	35	55.0	590	11.9
6	60.0	598	12.6	36	60.0	600	12.3
7	58.2	600	12.2	37	57.0	600	12.0
8	57.0	590	11.7	38	58.0	595	11.9
9	59.0	598	12.1	39	60.0	600	13.1
10	59.5	590	12.1	40	61.0	598	12.6
11	60.0	588	12.3	41	59.0	595	12.2
12	59.0	600	12.6	42	58.8	600	11.9
13	57.0	595	11.5	43	60.5	600	13.6
14	58.0	595	11.8	44	59.0	605	12.7
15	60.0	592	12.1	45	60.0	605	13.2
16	58.0	600	12.1	46	58.5	600	12.2
17	58.5	590	12.0	47	61.0	582	11.5
18	57.0	590	11.6	48	61.5	600	13.2
19	58.0	590	11.9	49	60.5	595	12.5
20	59.0	599	11.4	50	57.9	580	11.8
21	59.0	600	12.9	51	57.0	597	11.8
22	58.5	595	11.8	52	60.0	590	11.7
23	59.0	600	12.5	53	60.0	600	12.9
24	57.5	598	12.4	54	60.0	596	12.4
25	59.0	590	11.7	55	58.0	605	12.9
26	59.0	590	11.7	56	59.0	595	12.1
27	60.0	590	12.1	57	57.0	595	12.4
28	60.0	610	13.5	58	58.5	600	12.9
29	58.0	590	11.7	59	60.0	590	11.8
30	57.5	600	12.2	60	58.2	600	12.1
				Avg.	58.9	596	12.2

Table VII. Cell Characteristics of Lot T-7 Under 100 mW/cm^2 Tungsten Light

8 Hour Diffusion at 325°C on Czochralski Silicon							
Cell No. T-7	I_{sc} (mA)	V_{oc} (mV)	E_{ff} (%)	Cell No. T-7	I_{sc} (mA)	V_{oc} (mV)	E_{ff} (%)
1	58.5	580	11.4	31	56.6	585	11.5
2	59.3	590	12.1	32	57.0	600	13.0
3	58.5	590	12.1	33	59.0	590	11.2
4	60.0	585	11.9	34	56.0	590	11.5
5	60.1	590	11.9	35	58.0	595	12.4
6	59.0	590	11.9	36	54.0	595	11.9
7	58.0	580	11.2	37	56.0	580	10.9
8	57.2	590	11.8	38	58.0	591	11.4
9	58.0	585	11.6	39	56.8	590	11.9
10	57.5	589	11.7	40	60.0	590	12.2
11	59.0	580	11.2	41	59.0	580	11.0
12	61.0	590	11.5	42	57.5	582	11.8
13	58.0	590	11.8	43	57.2	595	12.7
14	57.0	582	11.2	44	50.9	592	11.2
15	61.0	590	12.2	45	60.0	581	11.4
16	58.8	582	11.7	46	57.9	585	11.5
17	60.0	580	11.2	47	56.5	573	11.0
18	59.0	590	12.2	48	58.5	585	11.0
19	59.0	585	11.9	49	57.0	590	11.8
20	59.1	585	12.2	50	58.8	585	11.8
21	59.8	595	13.0	51	59.0	592	12.1
22	58.0	598	12.5	52	60.0	595	12.8
23	57.0	570	10.3	53	56.0	590	11.5
24	58.5	600	13.0	54	57.9	595	12.4
25	59.9	580	12.9	55	58.0	584	11.3
26	58.0	589	11.1	56	60.0	585	11.9
27	57.0	590	11.5	57	54.8	589	11.8
28	57.8	580	11.3	58	57.5	572	11.2
29	58.5	595	12.2	59	59.5	598	12.6
30	58.8	592	12.0	60	60.3	588	12.0
				Avg.	58.2	588	11.8

Table VIII. Cell Characteristics of Lot T-8 Under 100 mW/cm^2 Tungsten Light

8 Hours at 325°C Diffusion on Whole Slices of Czochralski Silicon							
Cell No. T-8	I_{sc} (mA)	V_{oc} (mV)	E_{ff} (%)	Cell No. T-8	I_{sc} (mA)	V_{oc} (mV)	E_{ff} (%)
1	57.0	599	13.2	31	56.4	594	12.9
2	58.0	590	13.0	32	56.3	590	12.7
3	57.2	595	13.2	33	56.0	590	12.5
4	56.0	590	12.9	34	57.9	586	12.8
5	56.0	590	12.8	35	57.5	590	13.0
6	56.8	592	13.0	36	56.8	585	12.7
7	56.5	593	13.0	37	55.5	594	12.9
8	57.1	592	13.0	38	54.5	579	11.8
9	56.0	595	13.0	39	55.0	580	12.2
10	57.1	591	12.9	40	53.8	590	12.2
11	57.0	590	13.2	41	56.0	588	12.5
12	58.0	594	12.9	42	55.5	585	12.0
13	57.9	600	13.3	43	55.0	590	12.2
14	57.2	598	13.5	44	55.8	590	12.4
15	58.0	595	13.3	45	55.7	582	12.3
16	58.0	600	13.6	46	54.5	580	12.2
17	56.0	580	12.1	47	56.0	584	12.2
18	54.5	585	12.2	48	55.5	590	12.4
19	54.5	580	12.2	49	56.9	595	13.2
20	57.2	580	11.9	50	56.0	588	12.2
21	56.5	590	13.0	51	55.9	584	12.2
22	55.5	595	13.1	52	54.0	590	12.8
23	55.5	590	12.8	53	55.0	594	12.7
24	57.0	589	12.8	54	53.5	591	12.2
25	56.6	579	12.4	55	56.8	590	12.8
26	57.8	590	12.6	56	53.0	580	12.3
27	55.3	593	13.0	57	55.0	590	11.8
28	55.5	590	12.6	58	56.5	583	11.8
29	56.1	590	12.8	59	54.5	595	12.7
30	56.0	590	12.6	60	52.9	582	12.0
				Avg.	56.0	589	12.6

Table IX. Cell Characteristics of Lot T-9 Under 100 mW/cm^2 Tungsten Light

8 Hour Diffusion at 325°C on Whole Slices of *Lopex* Silicon							
Cell No. T-9	I_{sc} (mA)	V_{oc} (mV)	E_{ff} (%)	Cell No. T-9	I_{sc} (mA)	V_{oc} (mV)	E_{ff} (%)
1	54.0	600	12.8	31	55.0	590	12.0
2	54.0	587	11.5	32	56.0	600	13.0
3	52.5	600	12.0	33	54.0	599	12.5
4	54.5	598	12.5	34	55.0	597	12.5
5	54.0	600	12.6	35	55.5	600	13.0
6	56.5	602	13.5	36	54.5	592	12.5
7	56.2	595	12.5	37	56.0	600	13.2
8	55.2	600	13.0	38	55.0	600	12.8
9	55.2	600	13.0	39	54.9	600	12.9
10	54.5	600	12.5	40	55.4	600	12.5
11	55.0	600	13.1	41	55.8	602	13.0
12	54.1	601	12.9	42	55.2	600	12.6
13	56.0	600	13.2	43	54.5	595	12.5
14	55.5	592	12.6	44	54.5	600	12.8
15	55.8	600	12.9	45	54.5	598	12.5
16	56.2	600	12.8	46	55.5	600	12.9
17	55.0	590	12.5	47	54.6	600	13.0
18	55.1	600	13.1	48	55.0	595	12.8
19	55.0	603	13.3	49	55.0	601	13.2
20	55.8	600	12.8	50	58.2	595	13.1
21	57.0	585	12.0	51	58.3	600	13.5
22	54.5	595	12.0	52	57.0	600	13.4
23	54.5	600	12.6	53	58.0	595	13.1
24	54.8	595	12.5	54	56.8	600	13.3
25	54.0	602	12.8	55	56.2	598	12.8
26	55.1	601	13.2	56	55.2	594	12.0
27	55.9	600	13.0	57	56.0	584	11.9
28	54.1	600	12.5	58	52.8	596	12.4
29	54.0	595	12.2	59	54.1	592	12.0
30	54.5	600	12.8	60	52.8	600	12.1
				Avg.	55.2	598	12.7

Table X. Cell Characteristics of Lot T-10 Under 100 mW/cm^2 Tungsten Light

Double Boron Diffusion Depth 135 Minute Diffusion at 400°C on Whole Slices *Lopex* Silicon							
Cell No. T-10	I_{sc} (mA)	V_{oc} (mV)	E_{ff} (%)	Cell No. T-10	I_{sc} (mA)	V_{oc} (mV)	E_{ff} (%)
1	54.1	589	12.1	31	55.0	598	12.9
2	56.1	590	12.3	32	55.1	600	12.9
3	56.3	600	13.5	33	55.0	600	13.1
4	53.5	595	12.5	34	54.0	599	12.8
5	54.2	598	12.9	35	56.0	605	13.4
6	58.5	600	13.7	36	57.0	601	13.7
7	54.0	590	12.5	37	54.0	600	12.7
8	54.0	591	12.3	38	54.7	600	12.8
9	53.7	590	12.4	39	56.0	595	12.8
10	57.4	594	13.1	40	53.9	600	12.6
11	55.0	600	13.0	41	55.0	595	12.5
12	54.0	590	12.2	42	54.0	601	12.8
13	54.8	590	12.8	43	53.2	600	12.7
14	55.0	590	12.6	44	55.3	600	12.9
15	54.8	585	12.1	45	54.5	605	13.0
16	55.9	585	12.1	46	53.0	603	12.8
17	54.5	591	12.2	47	54.1	600	12.2
18	53.0	598	12.6	48	53.8	598	12.4
19	54.3	590	12.0	49	52.8	600	12.4
20	53.2	600	12.5	50	54.0	600	12.3
21	54.5	595	12.9	51	53.0	599	12.3
22	55.8	599	13.0	52	55.2	605	12.9
23	53.0	599	12.5	53	57.0	595	13.2
24	54.0	600	12.9	54	52.0	590	11.8
25	55.2	599	12.9	55	55.0	590	12.5
26	56.0	605	13.5	56	52.0	591	12.0
27	55.1	595	12.8	57	55.5	600	13.2
28	55.0	600	12.9	58	55.9	598	12.6
29	53.0	590	12.3	59	53.5	600	12.7
30	54.6	595	12.8	60	55.1	600	12.6
				Avg.	54.6	597	12.7